

**Design Optimization of Turbofan Engine for an Unmanned
Aerial Vehicle**

A Final Year Project Report

Presented to

SCHOOL OF MECHANICAL & MANUFACTURING ENGINEERING

Department of Mechanical Engineering

NUST

ISLAMABAD, PAKISTAN

In Partial Fulfillment
of the Requirements for the Degree of
Bachelors of Mechanical Engineering

by

Umer Saadat

Ateequllah Abid Zaka

Nafay Dar

Moazma Iftikhar



June 2020

EXAMINATION COMMITTEE

We hereby recommend that the final year project report prepared under our supervision by:

Umer Saadat	177437.
Nafay Dar	186248
Moazma Iftikhar	173854
Ateequllah Abid Zaka	187942

Titled: "Design Optimization of Turbofan Engine for an Unmanned Aerial Vehicle" be accepted in partial fulfillment of the requirements for the award of BACHELORS OF MECHANICAL ENGINEERING degree with grade _____

Supervisor: Dr. Emad Uddin, (HOD-Mechanical), SMME, NUST	 Dated: 13-Aug-2020
Committee Member: Dr. Samir Rehman, Assistant Professor SMME, NUST	Dated:
Committee Member: Dr. Jawad Aslam, Assistant Professor SMME, NUST	



(Head of Department)

13-AUG-2020

(Date)

COUNTERSIGNED

Dated: _____

(Dean / Principal)

ABSTRACT

Turbofan engines are one of the most widely used jet engines in aircraft propulsion. The word turbofan is derived from turbine fan. The turbofan engine uses the mechanical energy from the gas turbine to drive a large ducted fan to accelerate the air rearwards. As opposed to a conventional jet engine, a turbofan doesn't rely on the kinetic energy of the exhaust gases to generate thrust but depends on moving large volumes of air that is bypassed from the engine core, resulting in a more efficient engine performance. However, there are no commercially available small-scale turbofans for mini Unmanned Aerial Vehicles which are used for military and civil purposes. That need is either fulfilled by slow propeller driven UAVs or highly inefficient turbojet engines. Our project aims to address this market need in providing efficient small-scale turbofan engines for UAVs.

ACKNOWLEDGMENTS

Our team acknowledges the contribution of the engineers and scientists at NASA and Boeing who have laid the foundation for workings of the turbofan engines and gas turbines, the guidance and supervision of our project supervisor and faculty advisors and the efforts of all our teachers. We would also like to acknowledge our industry partner, Faisal Engineering Services, for sponsoring and financing the project as well as its further development into a commercial product.

COPYRIGHTS

The design and development of the Axial Fan and the Prototype Shroud, its properties and specifications, and all related material are the intellectual property of the student authors: UMER SAADAT, ATEEQULLAH ABID ZAKA, NAFAY DAR and MOAZMA IFTIKHAR, the institution: SCHOOL OF MECHANICAL AND MANUFACTURING ENGINEERING of the NATIONAL UNIVERSITY OF SCIENCES AND TECHNOLOGY, ISLAMABAD, and the industry sponsor: FAISAL ENGINEERING SERVICES PVT. LTD.

Any unauthorized use of the research, the design and all pertaining elements will result in copyright infringement of the material and the authors and involved parties will have every right to take legal action against the perpetrator/s.

ORIGINALITY REPORT

Match Overview			×
18%			
<			>
1	pdfs.semanticscholar.... Internet Source	2%	>
2	Submitted to Cranfield ... Student Paper	2%	>
3	dspace.lib.cranfield.ac.... Internet Source	1%	>
4	nptel.ac.in Internet Source	1%	>
5	www.j-mst.org Internet Source	1%	>
6	web.aeromech.usyd.ed... Internet Source	1%	>
7	Submitted to Engineers... Student Paper	1%	>

8	Sadraey, . "Wing Design... Publication	1%	>
9	Submitted to University... Student Paper	<1%	>
10	Submitted to Vaal Univ... Student Paper	<1%	>
11	Jack D. Mattingly. "Ele... Publication	<1%	>
12	Submitted to Glyndwr ... Student Paper	<1%	>
13	Submitted to Emirates ... Student Paper	<1%	>
14	archive.org Internet Source	<1%	>
15	Submitted to Rutgers U... Student Paper	<1%	>
16	Submitted to Edith Co... Student Paper	<1%	>
17	Submitted to Curtin Uni... Student Paper	<1%	>
18	Submitted to University... Student Paper	<1%	>
19	Submitted to The Unive... Student Paper	<1%	>
20	Submitted to North We... Student Paper	<1%	>
21	Submitted to Aston Uni... Student Paper	<1%	>

TABLE OF CONTENTS

ABSTRACT	ii
ACKNOWLEDGMENTS	iii
COPYRIGHTS	iv
ORIGINALITY REPORT	v
LIST OF TABLES	ix
LIST OF FIGURES	x
ABBREVIATIONS	xii
NOMENCLATURE	xii
CHAPTER 1: INTRODUCTION	1
1. Motivation	1
2. Need	1
3. Objectives	2
CHAPTER 2: LITERATURE REVIEW	3
1. Turbo-fan Engines	3

2. Blade Design	4
3. Blade Laws.....	12
4. Axial Flow Fans.....	18
5. Airfoil	19
6. Engine.....	31
CHAPTER 3: METHODOLOGY	32
1. Engine CAD Model	32
2. Atmospheric Properties	32
3. UAV Specifications	33
4. Fan design methodology	33
5. Generating the airfoils	38
6. Generating the fan blade	40
7. Shroud Design Improvements.....	43
Chapter 4: Results and Discussions	45
1. Design Calculations.....	45
2. CFD Flow Simulation	47
3. CFD Result of Fan Simulation.....	48
CHAPTER 5: CONCLUSION AND RECOMMENDATION.....	60

REFERENCES 62

APPENDIX I: AIR PROPERTIES AT DIFFERENT ALTITUDES..... 64

LIST OF TABLES

Table 1: Values for ϕ and ψ from actual fans	17
Table 2: Atmospheric Properties	32
Table 3: UAV Specifications	33
Table 4: Airfoil Specifications	36
Table 5: Blade Parameters	40
Table 6: Fan Design Data.....	42
Table 7: Fan Parameters Specifications	43
Table 8: Design Calculations	45
Table 9: Material Properties	54
Table 10: Stress and Deformation Analysis.....	59

LIST OF FIGURES

Figure 1.1: Standard Military UAV	1
Figure 2.1: Fan Velocity Triangles	5
Figure 2.2: Blade Pressure Distribution	6
Figure 2.3: Incoming Flow Deflection.....	7
Figure 2.4: Blade Placement	8
Figure 2.5: Stagger Angle	9
Figure 2.6: Deflection in blades	9
Figure 2.7: Angle of incidence.....	10
Figure 2.8: Fan Parameters	13
Figure 2.9: Radial Equilibrium Theory	14
Figure 2.10: Common Ducted Fan.....	19
Figure 2.11: Forces on an airfoil	20
Figure 2.12: Airfoil Geometric Parameters.....	22
Figure 2.13: NACA Airfoil Section.....	27
Figure 2.14: Effect on No of Blades on Fluid Flow.....	29
Figure 2.12: KingTech K-60 TP Engine	31
Figure 3.1: Engine CAD Model	32

Figure 3.2: Design Parameter of Rotor Blade	35
Figure 3.3: Tip and Root Airfoil	37
Figure 3.4: Tip View of Fan Blade	41
Figure 3.5: Isometric View of Fan Blade.....	41
Figure 3.6: Isometric View of Fan	41
Figure 3.7: Isometric View of Turbofan Engine Assembly	42
Figure 3.8: Isometric View of Turbofan Engine Assembly showing Exhaust Holes	43
Figure 4.1: Isometric & Front View of Ducted Fan & its Computational Domain... ..	48
Figure 4.2: Stress Causing Factors in Rotating Fan	51

ABBREVIATIONS

CFD	Computational Fluid Dynamics
CAD	Computer Aided Design

NOMENCLATURE

α	Angle of Attack/ Air Angle	m	Mass Flowrate
ω	Angular Velocity	r	Radius
W	Average Velocity	V	Relative Velocity
β	Blade Angle	U	Peripheral/Rotational Velocity
h	Blade Height	σ	Solidity
L	Blade Length	ξ	Stagger Angle
BHP	Brake Horse Power	P_s	Static Pressure
C	Chord	U_w	Whirl Velocity
S	Pitch	T	Temperature
θ	Camber (angle)	Q	Volume Flowrate
A	Cross Sectional Area	$P_{t t}$	Total Pressure
ϵ	Deflection (angle)	D	Time
ρ	Density	WC	Tip Diameter
δ	Deviation (angle)	PC	Water Column (Pressure Unit)
η	Efficiency	C_p	Power Consumption
H	Enthalpy	n	Pressure Coefficient
ϕ	Flow Coefficient	Υ	Number of Blades
ψ	Work Coefficient	Re	Specific Gravity
d	Hub Diameter	μ	Reynolds Number
i	Incidence Angle	ν	Dynamic Viscosity
C_L	Lift Coefficient	M	Kinematic Viscosity
C_D	Drag Coefficient		Mach Number

CHAPTER 1: INTRODUCTION

1. Motivation

Faisal Engineering Services, a Lahore based industry, has been developing UAV bodies for Pakistan Aeronautical Complex (PAC), Kamra, for a few years and wanted to produce a fully functional drone. For this purpose, Kingtech K-60TP, a turboprop engine was imported. However, the engine failed to provide the required thrust.

The industry sought consultancy from Dr. Emad, who proposed that the turboprop be converted into a turbofan engine, in line with a similar project carried out by NASA and Boeing.



Figure 1.1: Standard Military UAV.

2. Need

The project encompasses both military and civil use. The engine can be integrated with drones used for surveillance and offense and UAVs used for rescue and relief operations.

As of 2017, UAVs are among the fastest growing technologies on the globe and efficient engines targeted at this market not only have a huge business potential but are also critical for a sustainable environment.

Some of the target markets for UAVs are:

1. Military
2. Surveillance
3. Rescue
4. Relief
5. Logistics
6. Mapping

3. Objectives

Following the objectives for the project:

1. Design, Development and Analysis of Fan Blades for Turbofan Engine
2. Parametric Study and CFD Analysis of Shrouded Turbofan Engine
3. Fabrication of the designed Fan and Shroud
4. Testing of Turbofan Engine

CHAPTER 2: LITERATURE REVIEW

1. Turbo-fan Engines

Turbo-fans are a type of Gas turbine used in airplanes to generate thrust for propulsive purposes. Turbofans have a high thrust-to-weight ratio, high obtainable thrust levels along with good fuel efficiency. Turbo-fans generate thrust via two streams of hot fluid; the first stream of fluid is the one emanating from the nozzle after passing through the compressor, combustion chamber and the turbine. The thrust thus produced, is known as jet thrust, as it is produced similar to how a turbojet produces its thrust. The second stream is the one which by-passes the core of the engine and is exhausted through the nozzle. This thrust is known as the fan thrust as it is generated due to pressure difference created through the action of a fan. The fan itself is driven via a shaft and gear assembly connected to the turbine. The ratio of air streams (mass flow rates) bypassing the core and entering the core is known as the bypass ratio (BPR for short). Turbofans with a high bypass ratio produce majority of their thrust as fan thrust, since the mass flow rate bypassing the core is much greater than the one passing through the core. A higher BPR results in less fuel being consumed per unit thrust produced (lower specific fuel consumption). High bypass ratio turbofan engines hence, are today the almost exclusive powerplant of choice for medium and long haul commercial aircraft as they are capable of providing high thrust levels alongside good fuel efficiency. About 80% of a modern turbofan engine's thrust is

generated by the fan. In order to ensure low engine fuel consumption, it is required that the fan blades transfer mechanical shaft power from the turbine into thrust with the lowest possible amount of aerodynamic losses.

Since our engine was initially a turboprop, which we subsequently have converted into a ducted turbofan, it has a high bypass ratio. This is likely to have beneficial results on fuel efficiency and thrust generation.

2. Blade Design

2.1 Velocity Triangles

The Characterization of flow in an axial fan and the parameter explanation of flow features characterize an important portion of the fan design methodology. Terminologies employed in analysis and design of an axial fan and their interpretation is important for the researcher. This part focuses on the definition of the parameters that are used to illustrate the geometry of axial flow fans. The flow in an axial fan is essentially 3D, nevertheless as a first step towards the understanding of blade design, we consider the flow to be 2-Dimensional, which is not a baseless assumption as the change in radial component is usually unnoticeably small. Velocity triangles are a very important tool for flow visualization and help in geometrically depicting the actual and relative velocities in both the rotor stage and the stator stage of an axial fan and form the basis for fan design.

The rotation of the rotor adds the whirl velocity $U\theta$ or $V\theta$ component to the flow which is basically the tangential velocity. Exit absolute Velocity c_2 is the vector sum of the

tangential component and the axial component.

The whirl velocity V_θ represents energy that has been added to the air flow by the rotor in its operation. According to Euler work equation for Turbomachinery:

$$P = \dot{m} (C_{\theta 2} - C_{\theta 1}) * U$$

Here:

- \dot{m} is the mass flow rate
- U is the peripheral velocity of the blade.

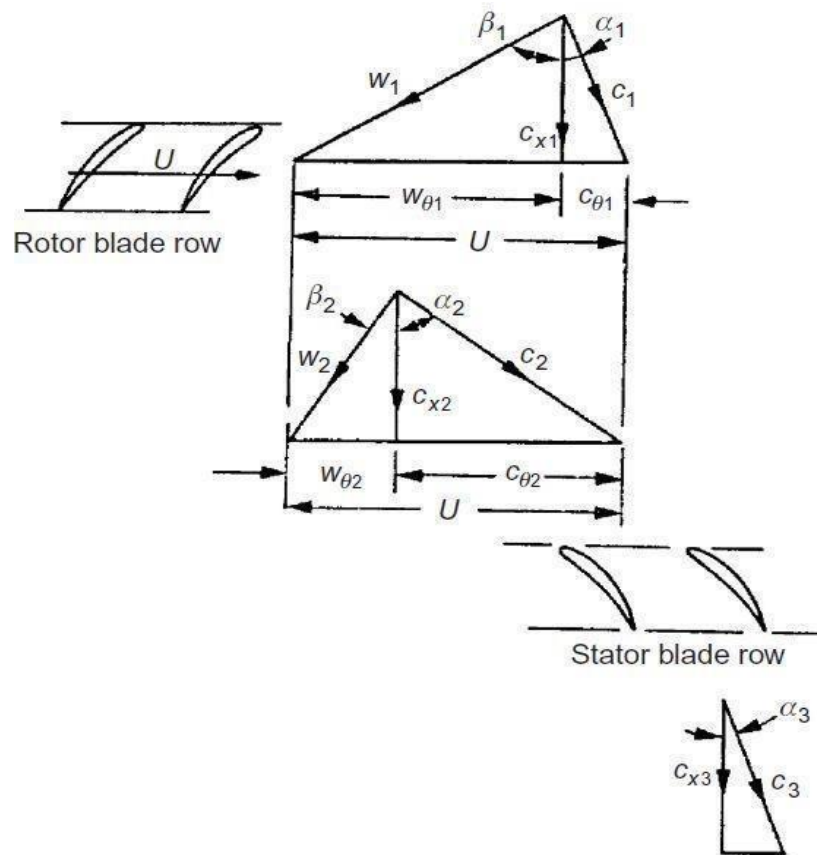


Figure 2.1: Fan Velocity Triangles [1].

2.2 DeHaller Number

DeHaller Number is the ratio of compression ratio and blade rotor (V_2/V_1). It describe to what extent on the rotor blade is relative velocity slows down.

To avoid boundary layer growth and wall stall DeHaller number should be greater than 0.72.

The flow start accelerating from the suction side and it reaches it's maximum value and then start decelerating. The decrement in acceleration is due to blade camber profile. [1].

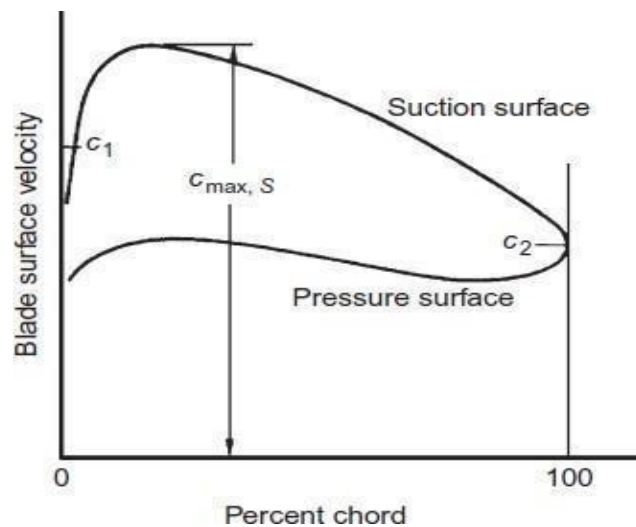


Figure 2.2: Blade Pressure Distribution.

2.3 Camber Change

Camber change is the difference of flow angle with which flow leaves blade β_2 and enter blade β_1 is called Camber Change denoted by ' $\Delta\beta$ '.

It is commonly known as incoming flow deflection.

$$\Delta\beta = \beta_2 - \beta_1$$

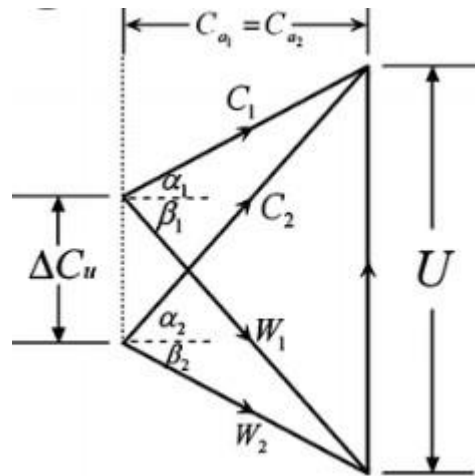


Figure 2.3: Incoming Flow Deflection.

2.4 Pitch

The measurement of distance around the hub between two similar point on consecutive blades is called fan blades pitch. Blade pitch angle is that angle at which blades are put relative to ground. The calculation of pitch is done by suitable radius length.

2.5 Chord

It is the imaginary straight line between the leading edge and the trailing edge. The magnitude of chord is greatest where wings join fuselage and the magnitude decreases towards the end of wing tip.

Chord of airfoil is represented in **Figure 2.3**

2.6 Solidity

Solidity is defined as ratio of Chord to Pitch and is directs the pressure rise and deflection. [McKenzie, 1997].

$$\sigma = C / (2 * \pi * r / n)$$

- r = radius of blade
- n = number of blades

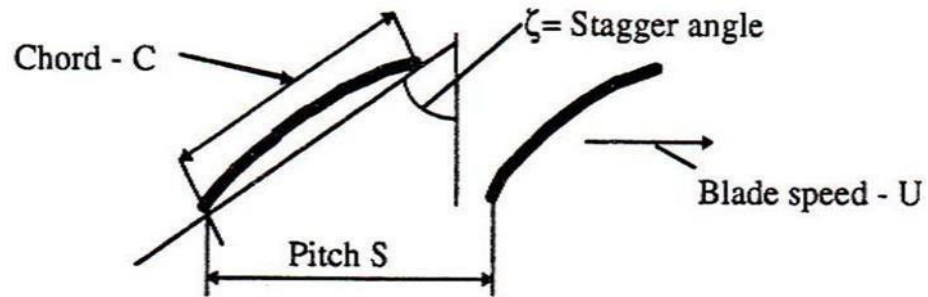


Figure 2.4.: Blade Placement.

The greater flow deflection and higher lift will be produced when blades are closed together due to consequent blades overlap and when blades are spaced sparsely, low flow deflection and lower lift will be generated.

Aerodynamically, solidity ratio should be greater than unity but at the same time for structural integrity, it should be less than unity. Common practice for selection of solidity ratio is unity.

2.7 Stagger Angle

Stagger angle (ξ) is the angle between chord line and axial axis of fan blades.

To achieve high pressure ratio, stagger angle should be increased and it should be as high as possible. The upper limit of stagger increase is controlled by blade overlap.

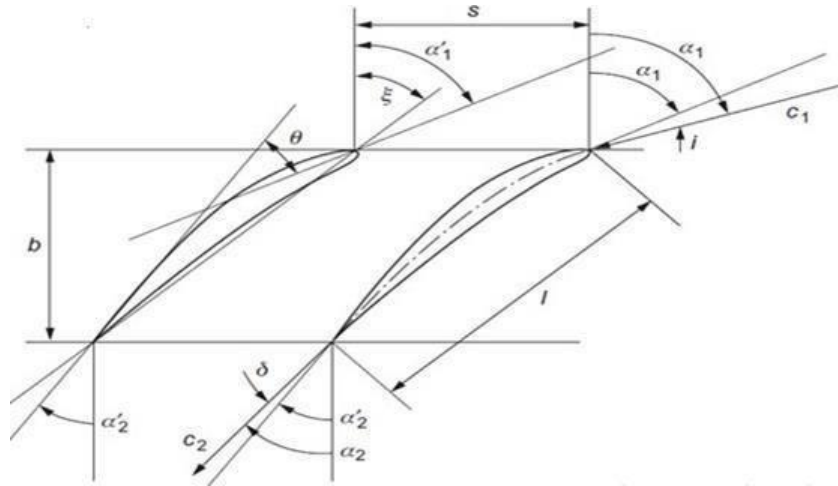


Figure 2.5: Stagger Angle.

However, increase in stagger angle for a given chord also increase the blade overlap and that resultantly reduces pressure rise. To overcome this, increase in chord can be a solution but diffusion due to restriction increase limit it. [2]

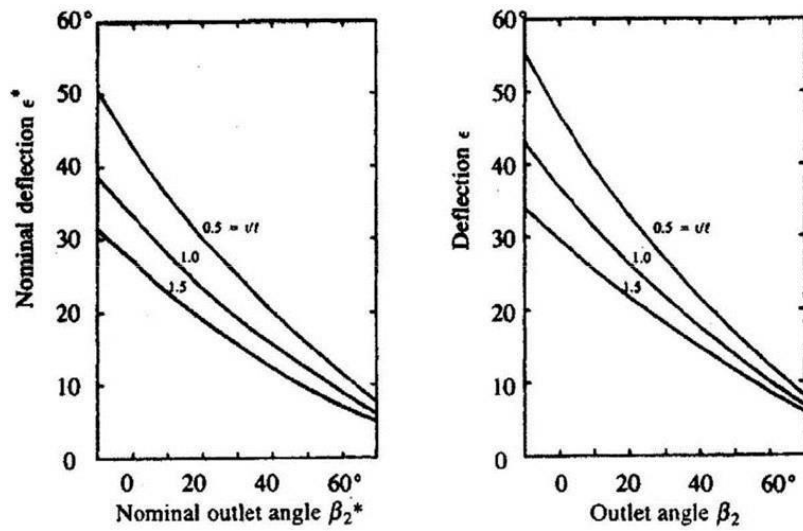


Figure 2.6: Deflection in blades

2.8 Setting Angle

Setting Angle (θ) is a measure of flow deflection. It is the change in relative flow angle at airfoil's leading edge and trailing edge.

2.9 Angle of Incidence

Angle of incidence is the difference between the blade angle at the leading edge β_1 , and the relative inlet velocity angle α_1 . Both angles are measured with respect to a horizontal line.

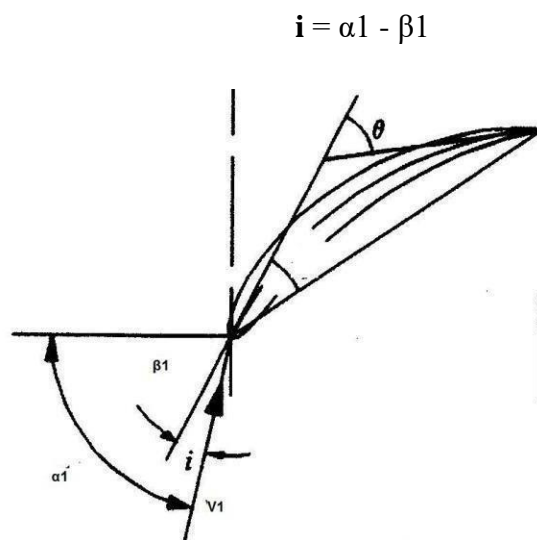


Figure 2.7: Angle of incidence.

Significance of incidence angle is that the flow division between suction surface and pressure depends on it. [3].

2.10 Fluid Deviation

Fluid deviation is the difference between the blade angle and the outflow angle.

$$\delta = \alpha_2 - \beta_2$$

2.11 Tip Clearance

The clearance between the shroud and the tip of the blade. The performance of blade and growth of boundary layer directly depends on tip clearance. It can be adjusted via blade height.

2.12 Fan Efficiency

Fan efficiency is defined as the ratio of aerodynamic power as output to mechanical shaft power as input. Total efficiency of fan can also be represented by the ratio of whirl component delivered to flowing air to shaft input. [2]

2.13 Degree of Reaction

The measure of rotor contribution in overall pressure rise in the stage is termed as degree of reaction. It is calculated by rise in stage's static pressure divided by rise in stage's total pressure.

The Degree of reaction usually varies considerably from hub to tip and usually increases radially [1].

2.14 Fan Total Pressure

Fan total pressure is the difference between the total pressures at the Fan Outlet and Inlet

[2].

2.15 Fan Velocity Pressure

It is the pressure corresponding to the average velocity at the fan outlet [2].

2.16 Total Pressure

It is a sum of Static Pressure and Velocity Pressure.

$$P_t = P_s + 1/2 * \rho * V^2$$

3. Blade Laws

The fan performance is described using the following three parameters:

- Volumetric flow rate
- Pressure rise
- Power consumption

A fan is designed to operate under specific conditions but its performance at off-design conditions can be predicted by these following fan laws:

3.1. Volumetric Flow Q

Volumetric flow for a fan is directly proportional to fan's rotational speed and the cube of fan diameter: $Q \propto N * D^3$

3.2. Pressure P

Static pressure is directly proportional to the square of fan rotational speed, diameter squared and density of the flowing air: $P_{st} \propto N^2 * D^2 * \rho$

3.3. Power Consumption PC

Power consumption is directly proportional to the cube of the rotational speed with fifth power of diameter and density of the flowing air: $PC \propto N^3 * D^5 * \rho$

The efficiency essentially remains similar and has a similar trend for all volumetric flow regimes.

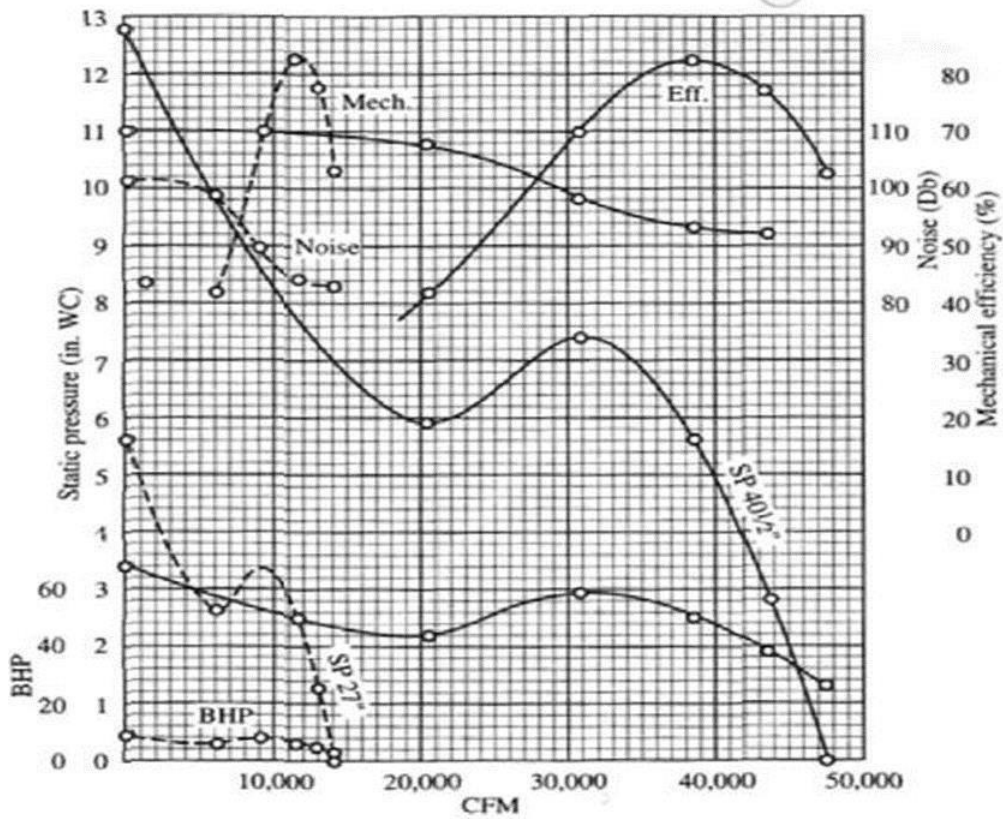
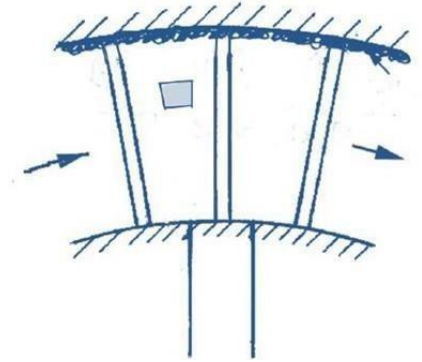


Figure 2.8: Fan Parameters [4].

3.4. Radial Equilibrium Theory

Consider a small element of fluid in between two blades which represents the fluid motion inside a rotor.



Initial assumptions:

- 1) Radial forces equilibrium governs the radial flow
- 2) radial flow occurs within the blades only
- 3) Gravitational forces are neglected

Consider an element subtended by an angle $d\theta$ of thickness dr along which the pressure variation is from p to $p+dp$. Resolving all the aerodynamic forces acting on this element in the radial direction, we get,

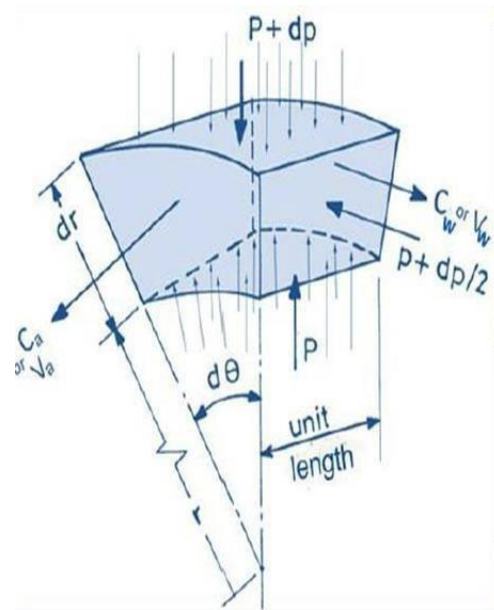


Figure 2.9: Radial Equilibrium Theory.

$$(p+dp) (r+dr) \cdot d\theta \cdot 1 - p \cdot r \cdot 1 \cdot d\theta - 2 (p+dp/2) \cdot dr \cdot (d\theta/2) \cdot 1 = \rho \cdot dr \cdot r \cdot d\theta Cw^2/r$$

By neglecting the higher order terms, the equation becomes

$$\frac{1}{\rho r} \frac{d}{dr} (r C_w^2) = \frac{C_w^2}{r}$$

This is called the Simple Radial Equilibrium Equation.

Using the following ideal equations:

1. $H = h + C^2/2 = C_p T + 1/2(Ca^2 + Cw^2)$ Energy Equation

2. $C_p T = \frac{d}{\rho} * \frac{\gamma}{\gamma-1}$ Equation of State

3. $P / \rho^\gamma = c$ Isentropic Law

Substituting Cp from eq 2 in eq 1 and differentiating it with respect to r yields

$$\frac{dH}{dr} = Ca * \frac{dCa}{dr} + Cw * \frac{dCw}{dr} + \frac{\gamma}{\gamma-1} [dp - \frac{pdp}{\rho^2}] \quad \text{-----(4)}$$

Differentiating eq 3

$$\frac{d\rho}{dr} = \rho \frac{dp}{\gamma p dr}$$

Substituting this in eq 4

$$\frac{dH}{dr} = Ca * \frac{dCa}{dr} + Cw * \frac{dCw}{dr} + \frac{dp}{\rho dr}$$

From simple radial equilibrium theory, we get:

$$\frac{dH}{dr} = Ca * \frac{dCa}{dr} + Cw * \frac{dCw}{dr} + \frac{Cw^2}{r}$$

H(r) = constant. As work distribution radially is constant:

$$\frac{dH}{dr} = 0$$

Thus, the energy equation can be written as:

$$C_a * \frac{dC_a}{dr} + C_w * \frac{dC_w}{dr} + \frac{C_w^2}{r} = 0$$

Now, if $C_a = \text{constant}$ at all radii, then the first term is zero and above equation reduces to:

$$C_w * \frac{dC_w}{dr} = - \frac{C_w^2}{r}$$

$$\frac{dC_w}{dr} = - \frac{dr}{r}$$

On integration, the equation becomes $C_w \cdot r = \text{constant}$.

This is known as the **Free Vortex Law**.

The generalized law for three-dimensional blade design takes the following form:

$$C_w \cdot r^n = \text{constant, where } -1 < n < 2$$

3.5. Flow Coefficient Φ and Work Coefficient Ψ

In order to compare fans on a standardized platform, two dimensionless parameters are defined, so instead of comparing fans on the basis of size, static pressure or flow variables, these parameters i.e. flow coefficient and work coefficient are used. Preliminary fan design requires the use of these dimensionless parameters to define a base fan design.

The flow coefficient is directly related to fan size, peripheral rotational speed and volumetric flow rate. The definition of the Flow Coefficient ϕ is [1, 2, 5]

$$\text{Flow Coefficient, } \phi = \frac{m/\rho A}{U}$$

The work coefficient directly relates pressure rise with dynamic velocity. The magnitude of this coefficient represents the pressure rise capability of the fan.

$$\psi = \frac{\Delta P}{\frac{1}{2} * \rho * U^2}$$

Both the flow coefficient and the work coefficient are directly related to the shape of the velocity triangle.

Table 1 illustrates the values of flow coefficient and work coefficient for market available fans as found in literature.

Design source	ν	ϕ	ψ	η	
A1	0.33	0.198	0.044	78%	} upstream guide vanes
A2	0.33	0.180	0.086	79%	
A3	0.47	0.230	0.16	84%	
A4	0.7	0.365	0.50	77%	
B	0.5	0.25	0.30	85%	} downstream guide vanes
C1	0.45	0.277	0.38	86%	
C2	0.5	0.268	0.52	85%	} no guide vanes
D1	0.5	0.244	0.155	78%	
D2	0.25	0.17	0.11	84%	} downstream guide vanes
E	0.55	0.145	0.25	86%	
F	0.55	0.225	0.24	79%	
G	0.50	0.203	0.49	75%	} contra-rotating

Table 1: Values for ϕ and ψ from actual fans [4].

For compressible high-speed flow, the work coefficient is given by,

$$\psi = \frac{\Delta H}{U^2}$$

$$\Delta h_0 = U * (C_{\theta 2} - C_{\theta 1})$$

$$\psi = \frac{(C_{\theta 2} - C_{\theta 1})}{U}$$

Following has been deduced for Axial Fans without guide vanes [1, 2, 3]:

Flow coefficient ϕ : 0.17 - 0.24

Work coefficient ψ : 0.11 - 0.15

The dimensionless parameters have the following effect on fan design [6]:

- Maximizing the product of flow coefficient and work coefficient yields a fan with maximum flow rate and a minimum size.
- Maximizing the work coefficient yield larger pressure rise and least noise.
- Maximizing the flow coefficient yields maximum flow capacity.

4. Axial Flow Fans

Fans in which the exit flow is perpendicular to exit plane and parallel to the axis of the rotor shaft is known as an axial fan. Axial fans are basically used for shifting high volume flow rates of fluid at relatively high speed with low pressure. Axial fans are used in small home appliances as well as in large HVAC units and airplanes. Due to their wide ranging

use, fan blade design becomes an integral part in differentiating axial fans for different application.

For our project, we will design a tube axial fan, which is also known as a ducted fan. A common design is shown in the figure. It will act as a turbofan when mounted on the engine shaft and enclosed in a shroud.



Figure 2.10: Common Ducted Fan

5. Airfoil

An Airfoil is the cross-section of an airplane's wings as well as fan and propeller blades. The motion of an airfoil through a fluid i.e. air produces aerodynamic forces due to the unique shape of the airfoil. Forces acting on an airfoil can be resolved along an x-y coordinate system and be classified as follows:

- Thrust – Towards the direction of motion
- Drag – Opposite the direction of motion
- Lift – Perpendicular to thrust in the upward direction

- Weight – Acting downwards due to gravity

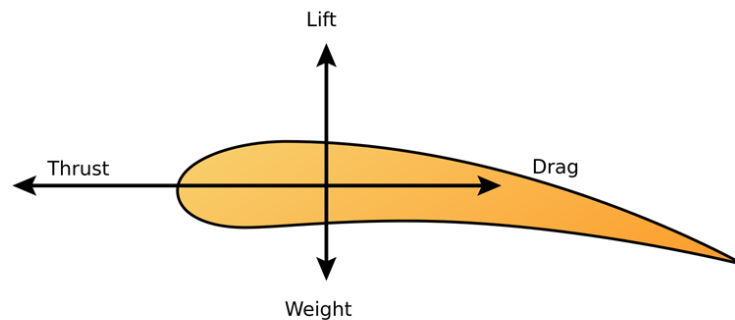


Figure 2.11: Forces on airfoil

An airfoil, when moved through air, experiences changes in static pressure on the top surface and on the bottom surface of the airfoil. This is because the geometric profile of an airfoil is such that the number of molecules colliding on the top surface is different from those colliding on the surface beneath. An airfoil section shown in figure 5.5, highlights the geometric design parameters of an airfoil.

The convex or upper surface of the airfoil is characterized by higher air velocity and low static pressure. Whereas, the concave or lower surface has relatively low air velocity and high pressure. This difference in pressures generate lift and is the principal behind flight and propeller blade motion. Thrust is also generated as a result of Newton's Third Law of motion.

The front edge where the air strikes first is called the **Leading Edge** and the other end is called the **Trailing Edge**. The straight line joining the leading and trailing edges of the

airfoil is known as the **Chord Line** and its length represents the width or span of the wing or blade. **Camber Line** shows the curvature of airfoil and maximum value occurs where the camber line is farthest from the chord line. Air comes into contact with the chord line of the airfoil at an angle. The angle between the relative air velocity and the chord line is known as **Angle of Attack α** .

If the mean camber line is a straight line, and the curves are mirror images of each other about the camber line, the airfoil is a symmetric airfoil. Symmetric airfoils, theoretically produce no lift as they do not produce any substantial pressure difference between the top and bottom profiles. The mean camber-line therefore, is generally not a straight line. Most airfoils have a positive camber as in that case, the upper surface experiences a static pressure that is less than the surrounding atmospheric pressure, while the lower surface experiences a static pressure higher than atmospheric pressure. This is due to a higher airspeed over the upper surface of the airfoil compared to that over the lower surface of the airfoil (refer figure 5.6 and 5.7). Increasing the **angle of attack**, creates a greater pressure difference between upper and lower surfaces. However, an angle of attack greater than a certain angle results in the separation of flow and vortex formation which can seriously increase drag and can also result in stalling. A certain compromise must thus be made.

The fan blade has been designed such that the leading edge is bend downwards to create a suction on blade's top area so that air always moves inwards of the engine and that too at a greater speed than before. Furthermore, the trailing edge is designed such that it is bent upwards so that when the air from the leading edge comes in with a high velocity it

not only compresses on the tip of the blade but also on the trailing edge. The angle the chord line connecting the leading and trailing edges makes with the horizontal axis is known as the **Setting Angle Θ** . Streamlines tend to maintain their position and due to the setting angle we have provided the streamlines get close to each other as they approach the trailing edge, creating a compressing effect and also increasing the velocity at the trailing edge. Again, the angle is kept such that the angle of attack does not exceed a certain value so as not to cause separation of flow and back flow

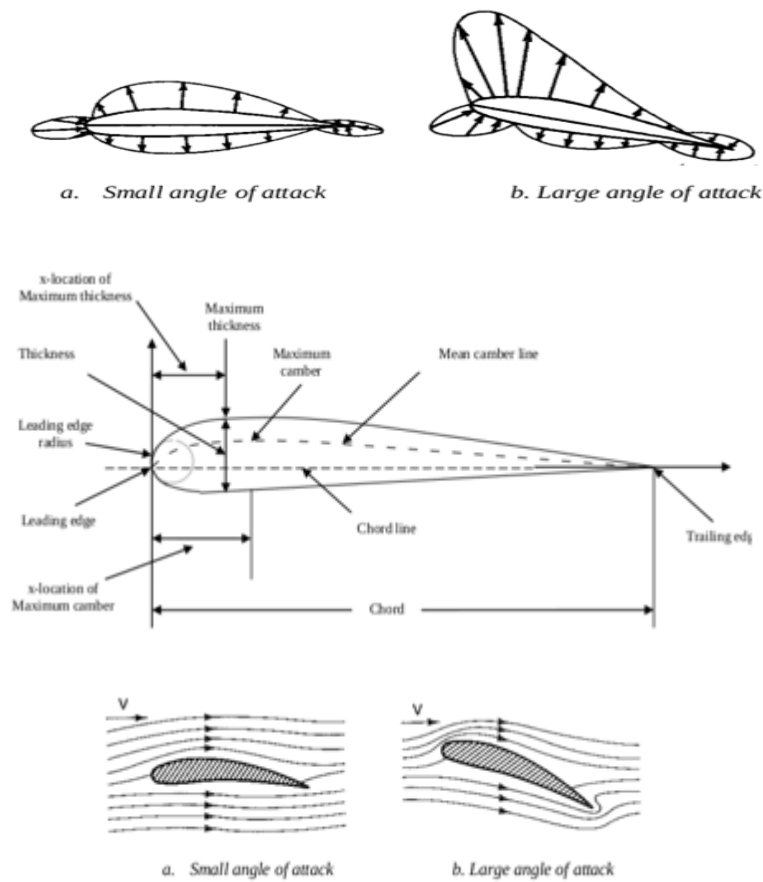


Figure 2.12: Airfoil Geometric Parameters

5.1 Characteristic Graphs of an Airfoil(Blaho,1975)

As discussed, the angle of attack has a great effect on the performance of an airfoil. An airfoil must be designed so that it is capable of performing optimally in the range of angle of attacks it is likely to experience throughout its use. While the geometry and pressure distribution are important parameters in deciding the airfoil chosen for a certain application, they cannot be relied upon as the sole basis of airfoil selection. We further examine certain airfoil operational outputs that provide a clearer picture of whether the airfoil satisfies agreed upon design requirements. Several non-dimensionalized operational parameters exist and their graphs against the angle of attack can allow us to make a comparison between airfoils with different geometric parameters. Lift, drag force and pitching moment are some of the more common parameters that are non-dimensionalized and graphed against various angle of attacks. Lift, drag force and pitching moment can be non-dimensionalized as shown below.

$$C_l = \frac{l}{\frac{1}{2}\rho V^2 (C \times 1)}$$

$$C_d = \frac{d}{\frac{1}{2}\rho V^2 (C \times 1)}$$

$$C_m = \frac{m}{\frac{1}{2}\rho V^2 (C \times 1) \times C}$$

Where l is lift, d is drag, and m is pitching moment of a two-dimensional airfoil. (C x 1) is the area of an airfoil with chord C and unit span (b = 1).

To gain an understanding of the performance of an airfoil, the following graphs are generated;

1. The lift coefficient variation against angle of attack
2. The pitching moment coefficient variation against angle of attack
3. A plot between pitching moment variation and lift coefficient variation
4. Drag coefficient against lift coefficient
5. Lift-to-drag ratio variation against the angle of attack

The above graphs have several critical features which form the criteria for airfoil selection(De Ryck, 2008).

5.2 Airfoil Selection Criteria

The airfoil selected depends upon the selection criteria that is employed. The selection criteria is a collection of design requirements. Following are some of the selection criteria employed:

1. Airfoil selection on the basis of highest maximum lift coefficient ($C_{l \max}$).
2. Selecting an airfoil based on the lift coefficient that is closest to a certain determined design lift coefficient ($C_{l d}$ or $C_{l i}$) at different angle of attacks.
3. Selecting an airfoil with the minimum drag coefficient ($C_{d \min}$).
4. Selecting an airfoil with the highest lift-to-drag ratio ($(C_l/C_d) \max$).

5. Selecting an airfoil based on the highest lift curve gradient ($C_{l \text{ gradient}}$).
6. Selecting airfoils with low pitching moment coefficient (C_m).
7. Selecting an airfoil in which the stall quality varies gently rather than sharply in the stall region.
8. Selecting an airfoil that is structurally sound and capable of handling the highest pressure it is likely to experience during its operation.
9. Selecting an airfoil keeping in mind the ease in manufacturing. Airfoils can be extremely precise and may require a lot of time, money and a specialized manufacturer to manufacture properly.
10. Cost based selection.

A unique airfoil which provides optimum values for all of the above given criteria does not exist. A compromise needs to be reached on which design criteria is most important.

An airfoil may have the highest maximum lift coefficient $C_{l \text{ max}}$, but not the highest value of maximum lift to maximum drag ratio ;

$$\left(\frac{C_l}{C_d} \right)_{\text{max}}$$

A compromise must be made through a weighting process, in which certain design criteria are given a greater importance compared to others.

5.3 NACA Airfoils

Design of an air foil from scratch requires investigation of several theories to analyze the flow around an airfoil. But as it requires a great deal of time and effort so considering the time we had, we chose to use airfoil design equations as developed by the National Advisory Committee for Aeronautics (NACA) to design our airfoils.

Airfoils designed using NACA developed equations are one of the most reliable and widely used airfoils. NACA was established in 1915 before finally being dissolved in 1958 in favor of creating a new committee called **National Aeronautics and Space Administration, NASA.**

Following airfoils are widely used;

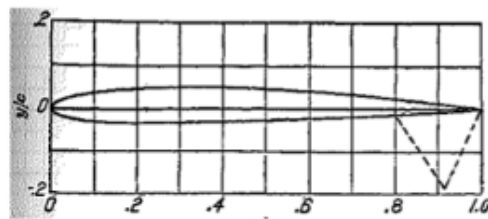
- Four-digit NACA airfoils
- Five-digit NACA airfoils
- 6-series NACA airfoil

Four-digit airfoil are represented using four digits (e.g, 1075) while five digit airfoils are represented by five digits (e.g,17869), while the 6-series airfoils are represented such that their name begins with the number six.

As in our project we'll be using the four-digit airfoil. Hence, in the literature review we'll be discussing in detail just the four-digit airfoil.

5.4 Four-digit NACA airfoils

In a Four-digit NACA airfoil, each digit represents a unique parameter or feature of the airfoil. The first digit represents the maximum camber as a percentage of chord length of the airfoil. The second digit represents the position of maximum camber in tenths of chord length (a 4 means the maximum camber occurs 40% along the chord line). The maximum thickness-to-chord ratio is represented by the last two digits. If the first digit is a 0 the airfoil is a symmetrical airfoil section. To explain the above, a NACA 5507 airfoil section (see figure 5.19a) has a 7 percent maximum thickness to chord ratio (max t/c) (the last two digits), its maximum camber is 5 percent of its chord length, and its maximum camber occurs at 50 percent along the chord length. Although NACA airfoils provide an easy reference to follow to produce airfoils, the airfoils are not specialized and may generate higher drag compared to new specially produced airfoils.



a. NACA 1408 airfoil section

Fig 2.13: NACA Airfoil Section

5.5 No of Blades:

The decision of how many number of blades are used is very essential for the optimal design. The following relation has been derived from various experimental studies to determine the number of blades to be used for the optimal functioning of the turbofan. The relation shows the dependence of the number of blades over the hub diameter of the turbofan. (Kumar & Bartaria, n.d.)

$$n_b = \frac{6r}{1-r}$$

The static pressure produced is proportional to the number of blades and the blade width.

Increasing the number of blades also increases the noise produced and increasing the width of blades is quite expensive, the hub becomes heavy and the structure is imbalanced.

Hence, neither the width nor the number of blades can be increased beyond a certain limit because of the above-mentioned problems.

The major place where the turbulence and noise is produced is leading and trailing edges of the blade, not over the surface.

For optimum efficiency and lower noise levels fewer while wider blades should be employed for the turbofan. However, it would not be optimal to keep fewer number of blades and increase the width of the blade to a great extent for then it would be quite expensive and the structure would be hard to balance.

In general, as a compromise between efficiency and cost, five to twelve blades are good practical solutions.

The efficiency decreases by increasing the number of blades in the turbofan, as the weight of the structure increases and greater power is required to run the blades. Moreover, with increasing the number of blades the fluid experiences passage losses due to the blades obstructing the flow and causing large skin friction drag. On the other hand, keeping very few blades results in fluid's head loss due to excessive circulatory flow loss as a result of backflow of fluid which hinders the fluid flow in the direction intended.[1] The phenomenon is shown in the Fig below.

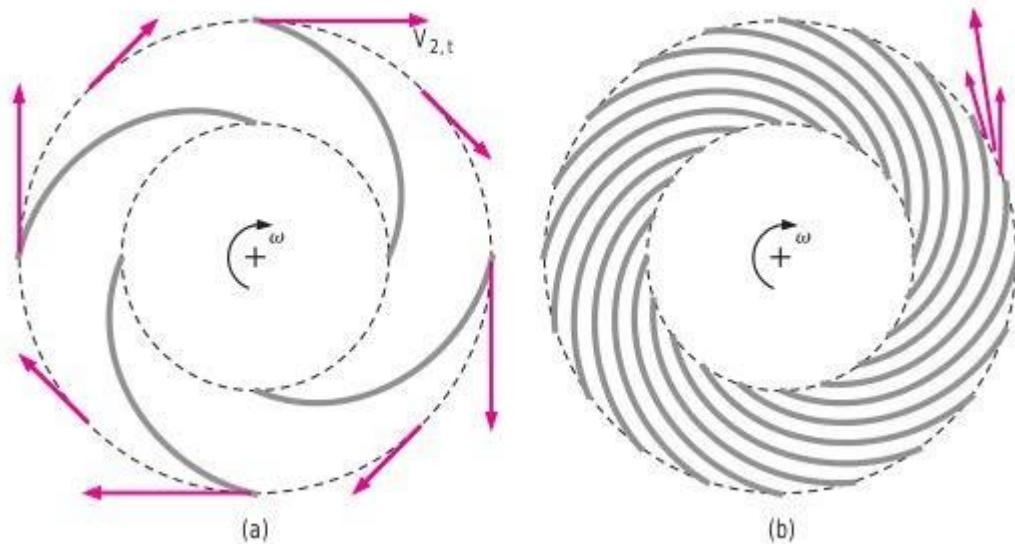


Fig 2.14: Effect on No of Blades on Fluid Flow

Medium sized fans are usually designed with 11, 14 and 16 number of rotor blades. (Kumar & Bartaria, n.d.)

Its concluded from experiments that for the small-sized fan 12 number of blades should be used that will keep the weight of the structure light, moreover, using 12 number of blades will keep both the circulatory flow losses and the passage losses within a bearable range.

5.6. Material Selection:

Among all the possible materials that are used for the design of fan blades the carbon fibre has the highest specific modulus elastic modulus. Hence, carbon fibre, for having high strength and low density(that is the unique feature of the composites and that differentiates it from other materials) as compared to other materials, is used for making the fan blades.

Material	Elastic Modulus	Tensile Strength
	Density (GPa/g · cm ⁻³)	Density (MPa/g · cm ⁻³)
Steel (AISI 4340)	25	230
Al (7075-T6)	25	180
Titanium (Ti-6Al-4V)	25	250
E Glass/Epoxy composite	21	490
S Glass/Epoxy composite	47	790
*Axamid/Epoxy composite	55	890
HS (High Tensile Strength) Carbon/Epoxy composite	92	780
HM (high modulus) Carbon/Epoxy composite	134	460

6. Engine:

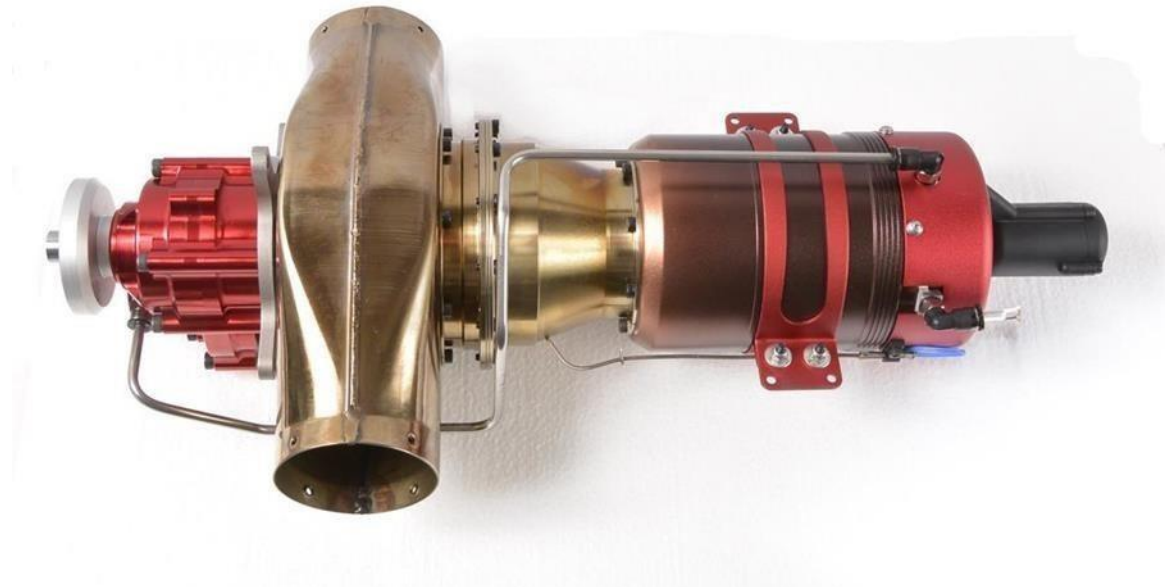


Figure 2.15: KingTech K-60 TP Engine [7]

CHAPTER 3: METHODOLOGY

1. Engine CAD Model

The CAD model of the KingTech K-60TP was generated using SolidWorks as shown in the figure below.

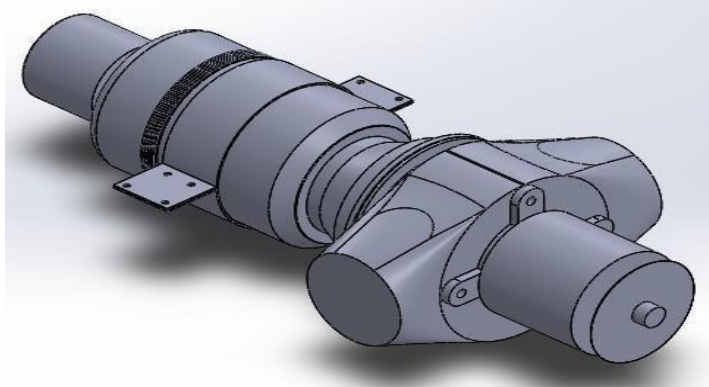


Figure 3.1: Engine CAD Model.

2. Atmospheric Properties

The reference values can be found in a table in Appendix I.

Properties	Sea Level	4572m
Temperature (°C)	15	-14.225
Gravity (m/s²)	9.807	9.793
Static Pressure (Pa)	101300	57850
Air Density (kg/m³)	1.225	0.7779
Dynamic Viscosity (x10⁻⁵ Ns/m²)	1.789	1.6445
Reynolds Number	326684	225679

Table 2: Atmosphere Properties

3. UAV Specifications

Altitude (m)	4572 (15,000 ft)
Cruise Speed (m/s)	97 (350 kph)

Table 3: UAV Specifications

4. Fan design methodology

There are two fan design methodologies, broadly speaking. They can be classified as;

i. Direct fan-blade design

In direct fan blade design we determine the efficiency, inlet and exit velocities, pressure differences when the operating conditions and the shape of the blade is provided. We can then parametrically achieve the highest possible efficiency.

ii. Inverse design methodology

In inverse methodology, we have an estimate of the air mass flow rate required and we then suitably apply parametric operation to achieve the desired flow rate or a flow rate near about.

Our objective is to maximize the thrust, and the engine is a turbo-fan. This obviously lends mass flow rate as the most important factor in thrust improvement. It suitably follows that we employ the Inverse Design Methodology to generate our fan design keeping in

mind a mass flow rate that will give us the required thrust. The shape of the designed fan-blade is regarded as being unknown and is controlled by a set of **design variables**; in addition, the desired volume flow rate of air for fan is considered available(Huang & Gau, 2012).

Through previous experimental results we assumed a required thrust of 75 N. Experimental results on previous design have yielded an optimum thrust equivalent to 59 N, hence the above estimate. Assuming an average velocity difference of 15ms^{-1} , the estimated mass flow rate turns out to be 5kg/s. Assuming the minimum $\rho = 0.7364 \text{ kg/m}^3$ at 5000m above the ground, we have an estimated maximum required air volume flow rate of $6.79 \text{ m}^3/\text{s}$ to maintain a thrust of 75 N at all altitudes.

5. Design variables

Selecting the proper design variables is very important for the formulation of the design problem. Essentially the design variables chosen are the ones which have the greatest effect on fan performance. A detailed literature review has helped us in narrowing down the variables investigated as follows;

- i) Four-digit NACA airfoil, root and tip (discussed in detail later)
- ii) Root chord length L_r
- iii) Tip chord length L_e
- iv) Setting angle Θ
- v) Twist angle ϕ
- vi) Number of fan blades
- vii) Hub diameter, Fan blade span or Aspect ratio

The figure highlights the parameters above (Huang & Gau, 2012);

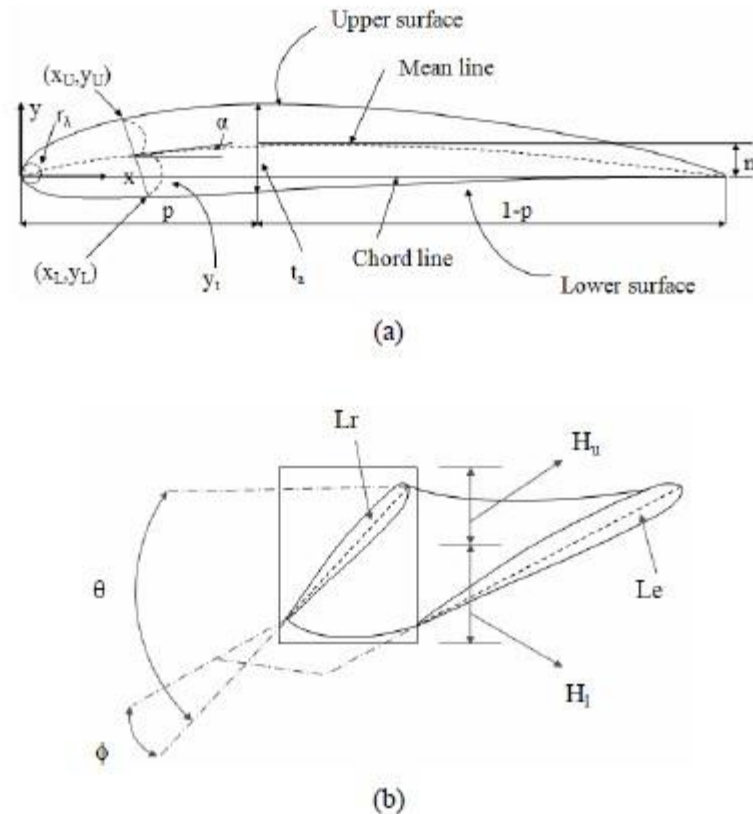


Fig. 1. The (a) geometric parameters of a two-dimensional NACA blade section; (b) design variables of the rotor blade.

Fig 3.2 : Design Parameter of Rotor Blade

Initially, it is desirable to designate more design variable than required and then slowly eliminate them by performing a sensitivity analysis. Each variable will be changed 5% of the original value while keeping the others constant and observing the effect on volume flow rate. If the effect of the variables on air flow rate is not significant, it is possible to assign a fixed numerical value to

those variables. Sensitivity analysis reduces the computer time involved in the design process. The above given design variables are iteratively varied and a CFD analysis is run to observe the thrust generated. The iterative design process is carried through till a thrust greater than 75 N is achieved. Our sensitivity analysis allowed us to assume twist angle and hub diameter as constants.

6. Airfoil design

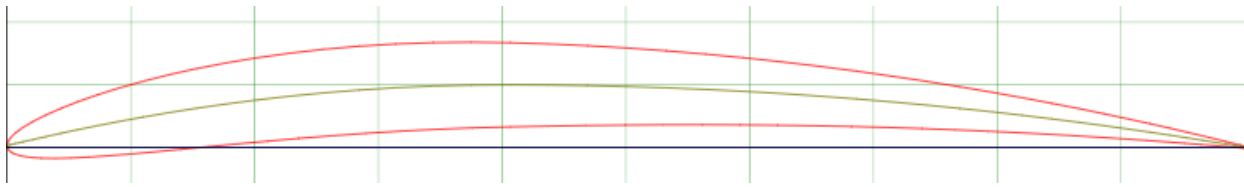
For the purpose of our fan we designed 2 NACA 4 digit airfoils; one for the root and the other for the fan tip (D. Almazo; C. Rodríguez; M. Toledo, 2013). Each digit of the 4-digit airfoil describes an aspect of the airfoil.

1. The first digit specifies the maximum camber of the airfoil as a percentage of the chord length of the airfoil.
2. The 2nd digit specifies the percentage distance along the chord where the maximum camber of the airfoil occurs.
3. The last two digits describe the maximum thickness of the airfoil as a percentage of the chord length.

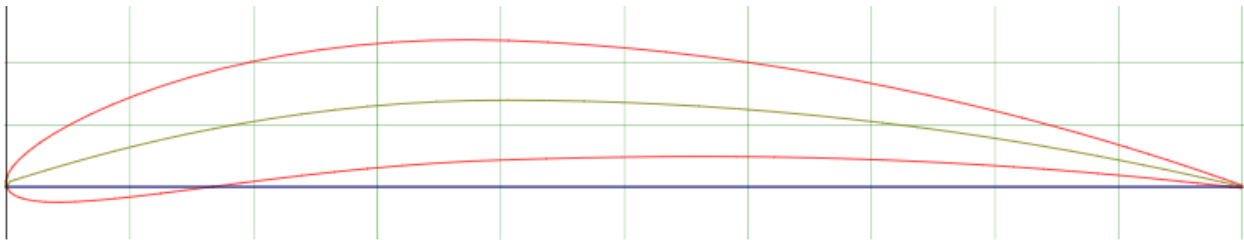
We iteratively found ourselves settling on the following airfoils. The below given airfoils achieved our design criterion (thrust greater than 75 N).

Airfoil	Max camber %	Max camber position %	Max thickness %	Airfoil Name
Tip	5	40	7	NACA-5407
Root	7	40	10	NACA-7410

Table 4 : Airfoil Specifications



Tip airfoil



Root Airfoil

Fig 3.3: Tip and Root Airfoils

The thought about selecting the various parameters is explained in the following sections.

Camber Percentage (m)

Having a higher maximum camber percentage makes the airfoil thicker. While this tends to make the airfoil less aerodynamic, a certain camber is required so that the fan blade can bear the stresses while operation. As the root is a stress concentration region with the greatest pressure stresses occurring there the max camber of the root airfoil (7%) is selected to be greatest. It progressively decreases along the span of the fan blade and is 5 % at the tip.

Max camber position (p)

Maximum camber position is an important parameter which controls the profile of the airfoil. It is

extremely necessary that the separation of flow is as little as possible during operation.

Selecting a maximum camber position that is 40% along the chord provides us with suitably aerodynamic airfoils.

Maximum thickness percentage (ta)

The maximum thickness percentage also determines the aerodynamics of the airfoil; again a compromise between good aerodynamics and stress resistance is required. Root airfoils are thicker than tip airfoils, hence the chosen values.

5. Generating the airfoils

The following is the procedure to generate the air foils.

Equations to generate air foil envelope $y =$

camber line position

$M =$ Maximum Camber %

$P =$ Maximum Camber position

$$y_{camber} := \left(\frac{M}{P^2} \right) (2 \cdot P \cdot x - x^2) \quad \text{from } 0 < x < P$$

$$y_{camber} := \left(\frac{M}{1 - P^2} \right) (1 - 2P + 2 \cdot P \cdot x - x^2) \quad \text{from } P < x < 1 \text{ To}$$

calculate the gradient of the camber line at each point;

$$gradient_{y_{cam}} := \left(2 \cdot \frac{M}{P^2} \right) (P - x) \quad \text{from } 0 < x < P$$

$$gradient_{y_{cam}} := \left(2 \cdot \frac{M}{(1-P)^2} \right) (P - x) \quad \text{from } P < x < 1$$

The thickness distribution is given by the equation:

$$y_t = \frac{T}{0.2} (a_0 x^{0.5} + a_1 x + a_2 x^2 + a_3 x^3 + a_4 x^4)$$

Where:

$$a_0 = 0.2969 \quad a_1 = -0.126 \quad a_2 = -0.3516 \quad a_3 = 0.2843$$

$$a_4 = -0.1015 \quad \text{or} \quad -0.1036 \quad \text{for a closed trailing edge}$$

The coefficients are for a maximum 20% thickness. T adjusts the equation for other thicknesses.

Note that y_t is half thickness; an equal thickness exists both sides of the camber line.

Once the camber line position, the gradient of the line at each position and the thickness at each position is calculated, we can find the position of the airfoil surface above and below the camber line as follows;

$$\theta = \text{atan} \left(\frac{dy_c}{dx} \right)$$

$$\text{Upper Surface} \quad x_u = x_c - y_t \sin(\theta) \quad y_u = y_c + y_t \cos(\theta)$$

$$\text{Lower Surface} \quad x_l = x_c + y_t \sin(\theta) \quad y_l = y_c - y_t \cos(\theta)$$

In order to make our airfoils we chose a hundred equally spaced values of x , and calculated the above camber line position, gradient at each position, the thickness at each position and the x and y coordinates of the surfaces above and below the camber line. All this gave us a series of points which we imported into SolidWorks to generate the airfoils.

6. Generating the fan blade

Once the airfoils had been generated, they were imported onto 2 separate planes 179mm apart. Since the imported airfoils were unit airfoils (1mm chord), they are suitably enlarged to achieve the desired root and tip chord lengths. Once enlarged, the airfoils are given suitable blade angles; that is the setting angle Θ and the twist angle ϕ . The root and tip airfoils are connected using a suitably twisted spline. In order to generate the spline, 4 control points were defined along the span of the fan blade. 3 of the control points were at positions 0%, 50% and 100% along the blade's span while the 4th control point was varied so as to provide additional control on generating the blade geometry (Chahine et al., 2015). The spline connecting the root and tip airfoils has been designed according to information gathered through literature review. The fan blade is generated by lofting the root airfoil along the spline trajectory till the tip airfoil. Again, like airfoil design, the blade angles are varied one at a time and their effect on thrust generated is observed before finally settling on the value which yields a thrust greater than 75 N. The following are the blade variables of the finalized blade design;

Root airfoil chord length L_r	82mm
Tip airfoil chord length L_e	50mm
Setting angle Θ	35 degrees
Twist angle ϕ	10 degrees

Table 5: Blade Parameters

Once the fan blade is generated, it is placed on top of a circular hub. The fan is completed by using the circular pattern tool in SolidWorks to create the required number of fan blades.

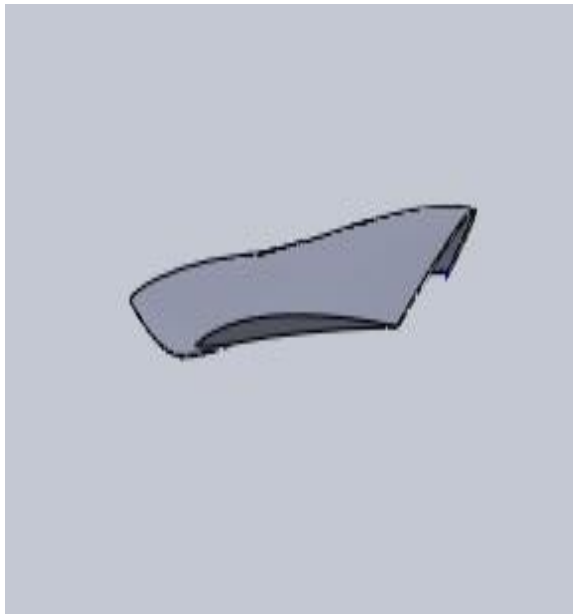


Fig 3.4: Tip View of Fan Blade

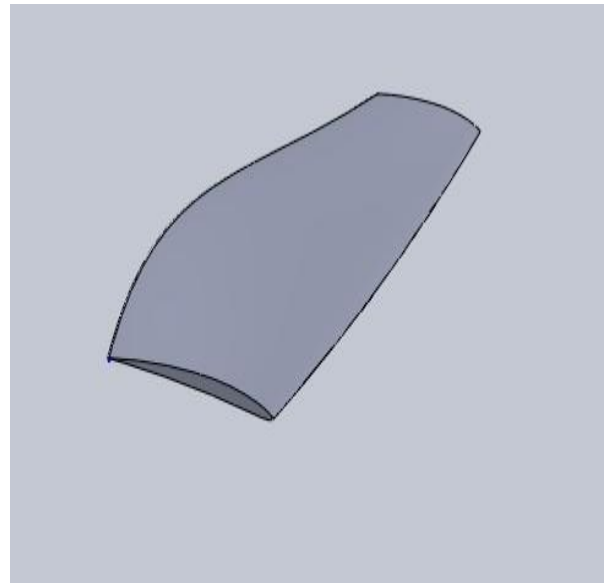


Fig 3.5: Isometric View of Fan Blade

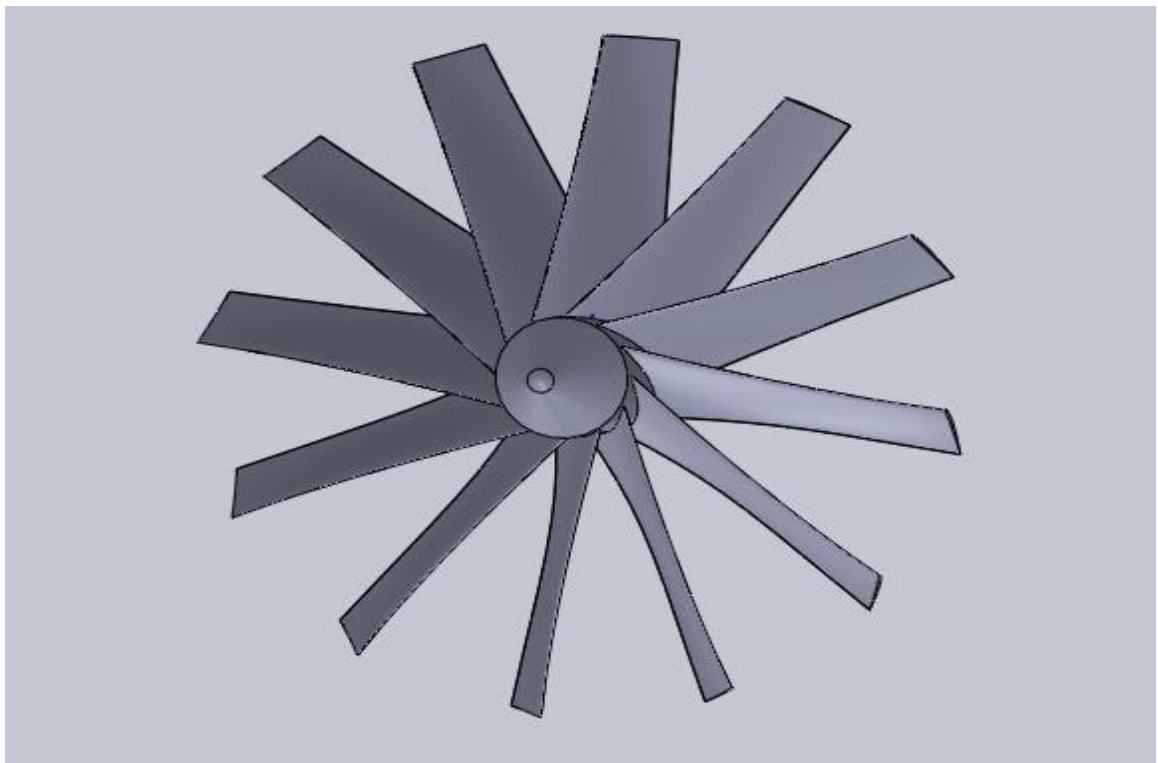


Fig 3.6: Isometric View of Fan

The results obtained for different fans generated have been tabulated in the table below;

	Original fan blade	Designed fan blade 1 (previous)	Designed fan blade 2	Final optimal fan blade
airfoil (tip)	GOE 474	AH 79-100B	5407	5407
airfoil (root)	GOE 474	E61	7410	7410
Blade root chord (mm)	70	49.87	82	82
Blade tip chord (mm)	40	49.87	50	50
Setting angle Θ	50	32.5	0	35
Blade twist angle	10	10	10	10
No. of fan blades	8	8	12	12
Fan speed (rpm)	7000	7000	7000	7000
Hub diameter (mm)	127	127	52	52
Fan diameter (mm)	410	410	410	410
Tip clearance (mm)	2	2	2	2
Thrust (N)	59	53	43	86

Table 6 : Fan Designs Data

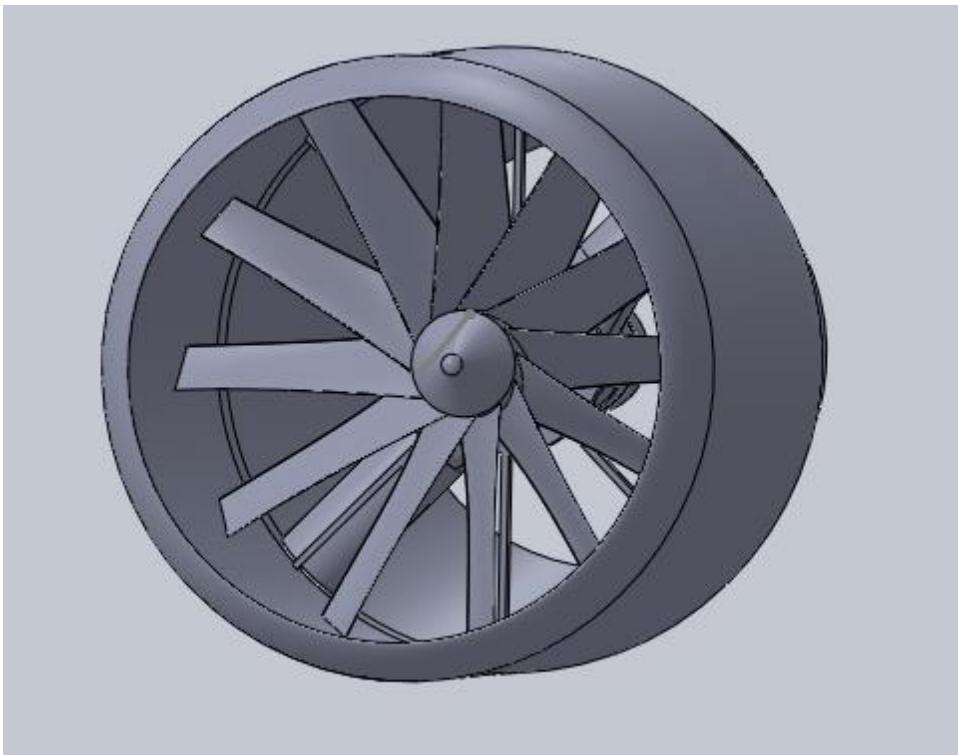


Fig 3.7: Isometric View of Turboman Engine Assembly

7. Shroud Design Improvements

A diffuser was designed at the shroud opening in order to decelerate the incoming air. In turn a nozzle was designed to accelerate the air exiting the shroud. Furthermore, 2 holes were created in the shroud so as to allow the exhaust tail pipes to be taken out of the shroud. The inlet diameter of the diffuser and the exit diameter of the nozzle were both 359.4mm.

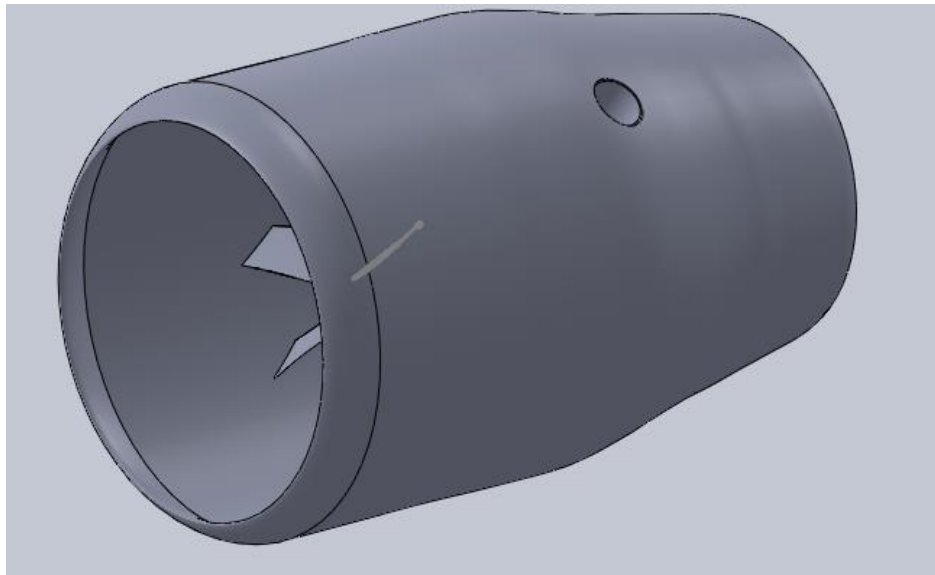


Fig 3.8: Isometric View of Turboman Engine Assembly showing Exhaust Holes

8. Fan parameter specifications

Tip Diameter	410 mm
Hub Diameter	52 mm
Fan Blade Span	179 mm
Aspect Ratio	2.18
Number of blades	12
Shroud Diameter	414 mm

Tip Clearance	2mm
Proposed Material	Carbon fiber
Maximum rpm (N)	7000
Assumed fan efficiency	90 %

Table 7: Fan Parameters Specifications

Chapter 4: Results and Discussions

1. Design Calculations

$$r_{tip} := 0.205 \text{ m}$$

$$\omega_{max} := 7000 \text{ rpm}$$

$$r_{root} := 0.026 \text{ m}$$

$$blade_angle := 35 \text{ deg}$$

$$u_{avg} := \frac{u_{tip} + u_{root}}{2} = 84.666 \frac{\text{m}}{\text{s}}$$

$$D := 0.410 \text{ m}$$

$$D_{hub} := 0.052 \text{ m}$$

$$Diff_dia := 0.39 \text{ m}$$

$$\rho := 0.7364 \frac{\text{kg}}{\text{m}^3}$$

$$\eta_{fan} := 0.9$$

$$power := 7300 \text{ W}$$

	Value
Tip Velocity (U_{tip})	$u_{tip} := r_{tip} \cdot \omega_{max} = 150.273 \frac{\text{m}}{\text{s}}$
Root Velocity (U_{root})	$u_{root} := r_{root} \cdot \omega_{max} = 19.059 \frac{\text{m}}{\text{s}}$
Air speed	$v_{axial} := u_{avg} \cdot \cos(blade_angle) = 69.354 \frac{\text{m}}{\text{s}}$
Chord Length	$Chord := \frac{Span}{A} = 0.082 \text{ m}$
Cross sectional area	$Area := \left(\frac{(D)^2 - (D_{hub})^2}{4} \right) \cdot \pi = 0.13 \text{ m}^2$
Diffuser Area	$Diffuser_inletArea := \frac{\pi \cdot Diff_dia^2}{4} = 0.119 \text{ m}^2$
V_{in}	$v_{in} := \frac{Diffuser_inletArea}{Area} \cdot v_{axial} = 63.779 \frac{\text{m}}{\text{s}}$
Minimum Mass flow rate	$mass_flow_rate := \rho \cdot (Area) \cdot v_{in} = 6.101 \frac{\text{kg}}{\text{s}}$

Volume flow rate	$volume_flow_rate := Area \cdot v_{in} = 8.285 \frac{m^3}{s}$
a (a parameter connecting v_{exit} and v_{in} in slipstream theory)	$a := \frac{1}{\eta_{fan}} - 1 = 0.111$
Velocity of air exiting fan	$V_{exit_fan} := (1 + 2 \cdot a) \cdot v_{axial} = 84.766 \frac{m}{s}$
Velocity of air exiting nozzle	$v_{exit} := \frac{Area}{Nozzle_exit_area} \cdot V_{exit_fan} = 92.176 \frac{m}{s}$
Thrust(theoretical) without nozzle and diffuser	$Thrust_{ideal} := mass_flow_rate \cdot (V_{exit_fan} - v_{axial}) = 94.03 N$
Change in air velocity	$velocity_change := \frac{power \cdot \eta_{fan}}{mass_flow_rate \cdot u_{avg}} = 12.719 \frac{m}{s}$
Flow coefficient, Φ	$flow_coefficient := \frac{volume_flow_rate}{Area \cdot u_{tip}} = 0.424$
Work coefficient, ϕ	$work_coefficient := \frac{velocity_change}{u_{tip}} = 0.085$

Table 8: Design Calculations

2. CFD Flow Simulation

The thrust calculations were performed using SolidWorks Flow Simulation. In the flow simulation the designed ducted fan is placed in a flow passage and air flows through it at a specified **Air Velocity**. **The flow has been assumed to be steady, incompressible and 3 dimensional**. The values of Static Pressure, Air Velocity and Rotational Speed were incorporated in the solver. The k- ϵ model has been used to model turbulence (Huang & Gau, 2012). The continuity and momentum equations for the problem are as follows;

$$\frac{\partial \rho \bar{u}_i}{\partial x_i} = 0, \quad (1)$$

$$\rho \bar{u}_j \frac{\partial \bar{u}_i}{\partial x_j} = -\frac{\partial \bar{p}}{\partial x_i} + \frac{\partial}{\partial x_j} \left[\mu_t \left(\frac{\partial \bar{u}_i}{\partial x_j} + \frac{\partial \bar{u}_j}{\partial x_i} \right) \right], \quad (2)$$

$$\rho \bar{u}_j \frac{\partial k}{\partial x_j} = \frac{\partial}{\partial x_j} \left(\frac{\mu_t}{\sigma_k} \frac{\partial k}{\partial x_j} \right) + \mu_t \left(\frac{\partial \bar{u}_i}{\partial x_j} + \frac{\partial \bar{u}_j}{\partial x_i} \right) \frac{\partial \bar{u}_i}{\partial x_j} - \rho \epsilon, \quad (3)$$

$$\rho \bar{u}_j \frac{\partial \epsilon}{\partial x_j} = \frac{\partial}{\partial x_j} \left(\frac{\mu_t}{\sigma_\epsilon} \frac{\partial \epsilon}{\partial x_j} \right) + C_1 \mu_t \frac{\epsilon'}{k} \left(\frac{\partial \bar{u}_i}{\partial x_j} + \frac{\partial \bar{u}_j}{\partial x_i} \right) \frac{\partial \bar{u}_i}{\partial x_j} - C_2 \rho \frac{\epsilon^2}{k}. \quad (4)$$

Since the fan is ducted the velocity at the walls and surfaces, u_i , is assumed to be 0 as per no slip condition. The inlet boundary type is chosen as inlet velocity and turbulence intensity as these parameters can be reasonably estimated before hand. The outlet boundary type is set as a pressure outlet. The above continuity and momentum equations are solved iteratively using the given boundary conditions by

the CFD solver till the error between two successive iterations is less than a specified value. Once the iterations are done, results for thrust are generated.

3. CFD Result of Fan Simulation:

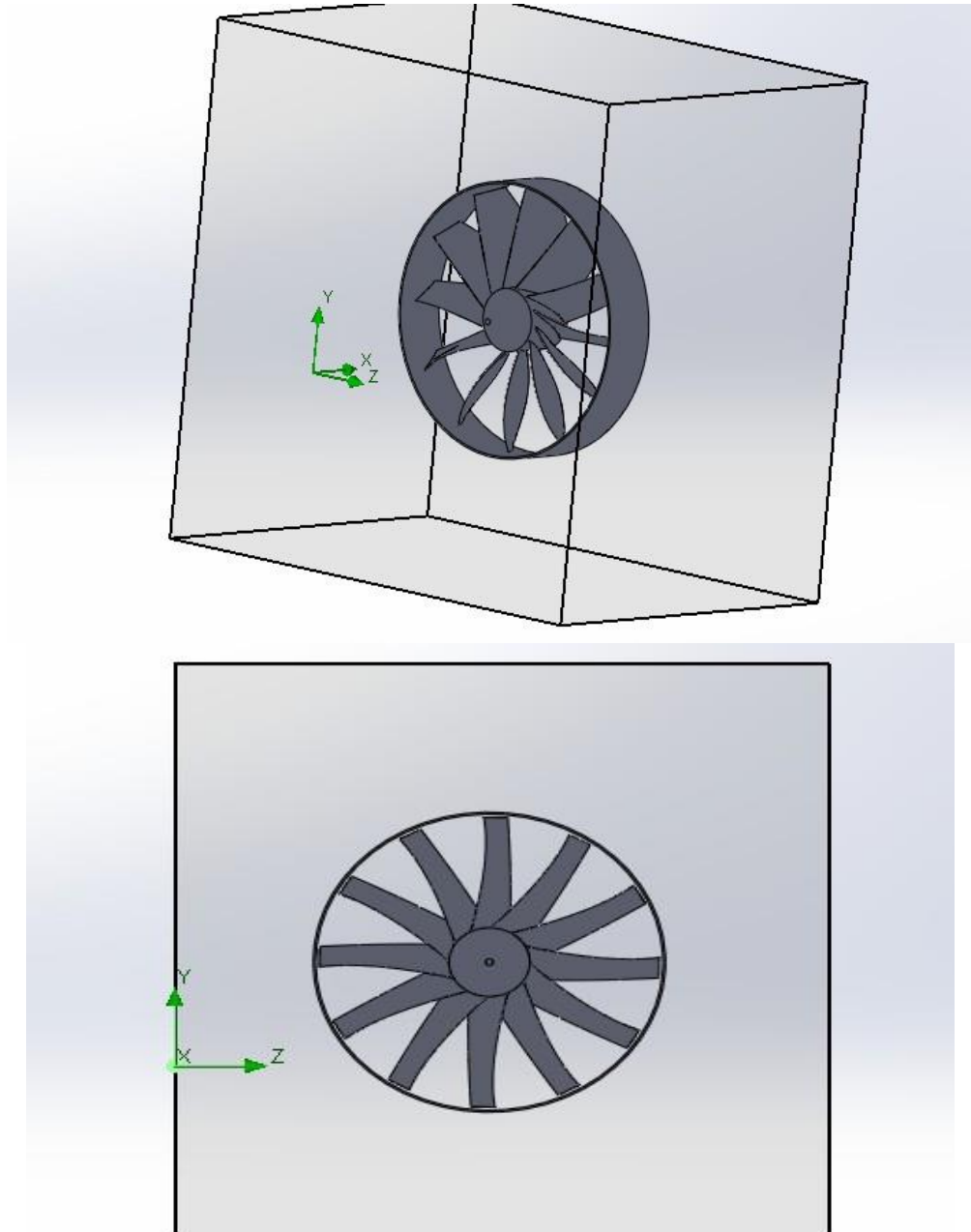


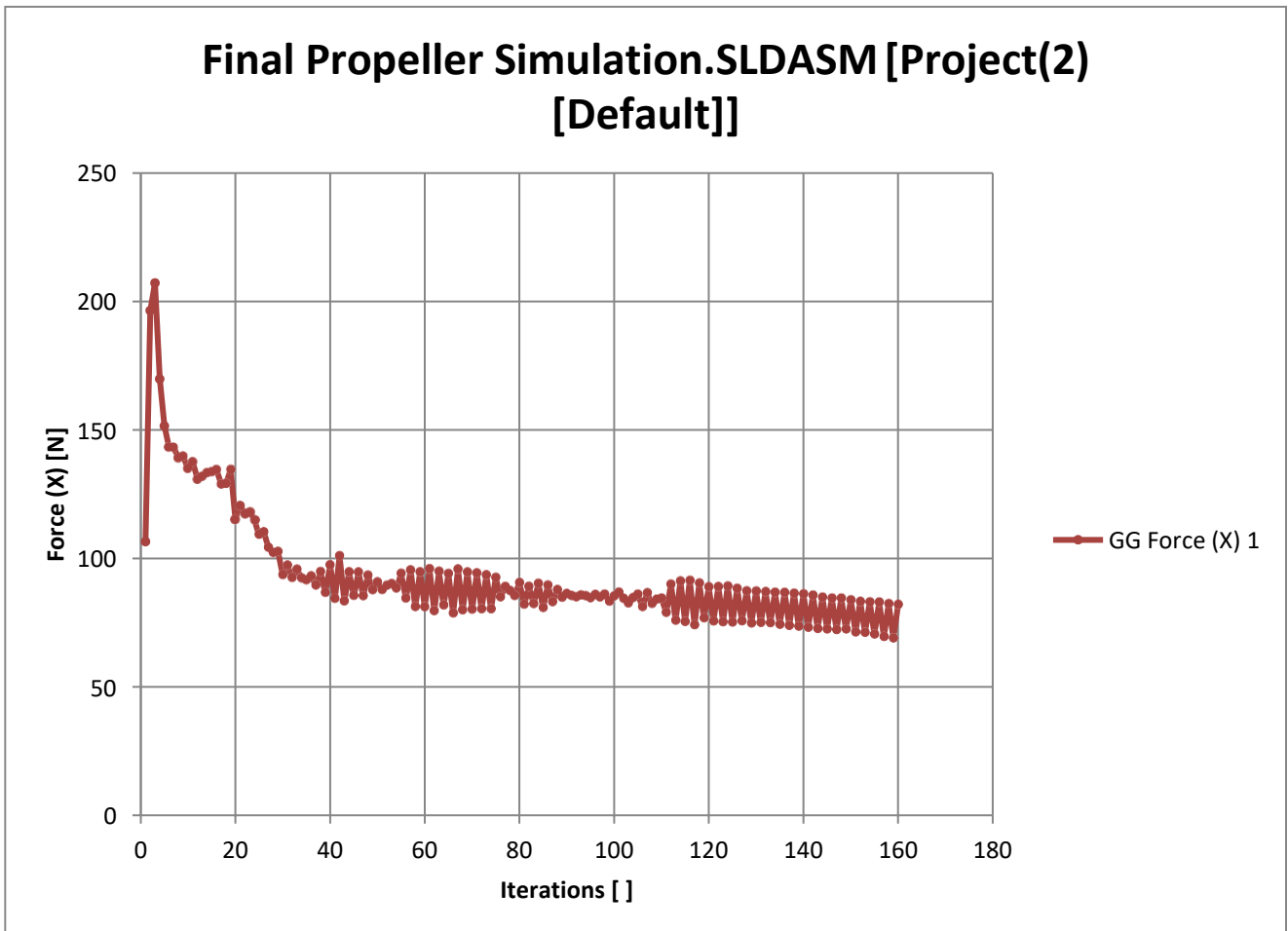
Fig 4.1: Isometric & Front view of the ducted fan and its computational domain

Density = 1.225

Goal Name	Unit	Value	Averaged Value	Minimum Value	Maximum Value	Progress [%]	Use In Convergence	Delta	Criteria
GG Force (X) 1	[N]	82.00416367	77.96819582	69.02818984	86.09716892	100	Yes	3.878647916	17.41692145
GG Force (Y) 1	[N]	-6.19373897	-3.708464237	-7.861121548	0.769539286	100	Yes	0.522447877	1.300150604
GG Force (Z) 1	[N]	3.35966787	3.051873533	2.095562021	3.704583239	100	Yes	0.137652952	0.97725847

Iterations []: 160
 Analysis interval: 21

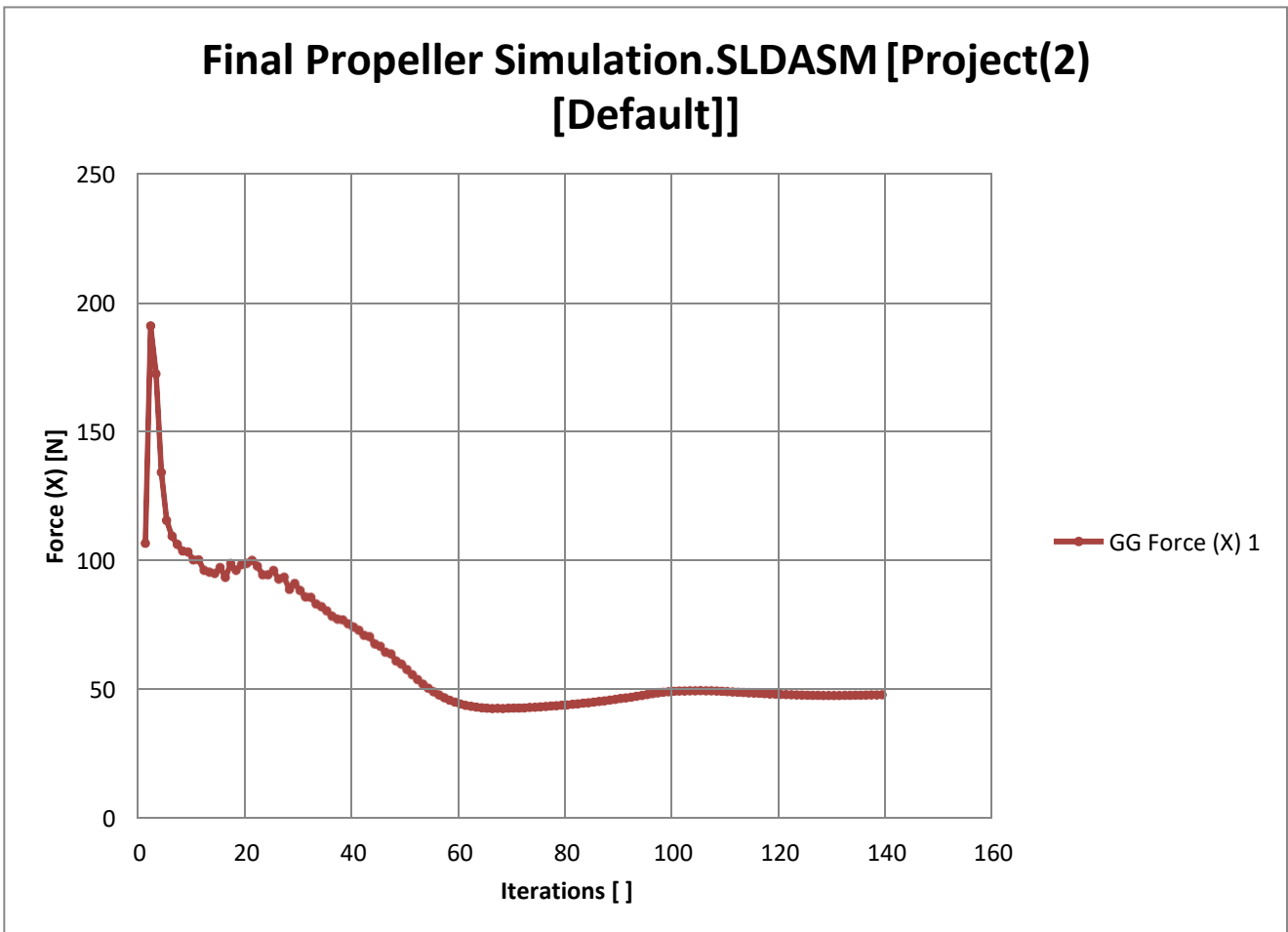
The result indicate the maximum thrust of 86.09 N and an average thrust value of 77.96 N.



Convergence plot of the fan thrust calculation simulation for $\rho=1.225 \text{ kg/m}^3$

Density = 0.7365									
Goal Name	Unit	Value	Averaged Value	Minimum Value	Maximum Value	Progress [%]	Use In Convergence	Delta	Criteria
GG Force (X) 1	[N]	47.96165545	47.83290617	47.65780471	48.19475433	100	Yes	0.536949621	14.15000396
GG Force (Y) 1	[N]	-3.42567298	-3.450403514	-3.487284384	-3.419375179	100	Yes	0.067909205	1.190283817
GG Force (Z) 1	[N]	2.443872948	2.422492461	2.356851372	2.474882086	100	Yes	0.047814754	0.786530756
Iterations []: 139									
Analysis interval: 21									

The result indicates a maximum thrust value of 48.19 N and an average thrust value of 47.83 N at a $\rho=0.7365 \text{ kg/m}^3$



Convergence plot for the thrust calculation simulation at $\rho=0.7365 \text{ kg/m}^3$

The drone is capable of flying at a maximum altitude of 4572m. The simulation has been performed at ground level as well as at an altitude of 5000m where the air density is minimum (0.7365kg/m^3). The thrust results for an altitude of 4572m can be reasonably assumed to be greater than those calculated in the simulation.

As can be seen, at ground level the maximum thrust generated is around 86 N. An altitude increases generally means a decrease in the density of air since less of the atmosphere lies above. As a result, though the volume flow rate of the turbofan remains the same, the mass flow rate decreases with the increase in altitude. Since the thrust of a turbofan is predominantly dependent on the mass flow rate of air, the thrust is likely to decrease with increase in altitude (decrease in density). This is exactly what is observed in the simulation results which predict a maximum thrust of around 48 N at an altitude of 5000m ($\rho=0.7365\text{ kg/m}^3$). At higher altitudes the need for thrust is lesser due to a lower drag force experienced as the air is less viscous than on the ground. Thus, a thrust value of 48 N is sufficient for altitudes between 4500-5000m.

Stress Analysis of Rotating Fan:

When a fan rotates the most predominant force it experiences is the centrifugal force which tends to pull the fan blade away from the hub. The centrifugal force, in turn also causes a turning moment. Another important force causing stress is the thrust force which tends to bend the fan blades forward. The force also results in a moment which tends to bend the fan blades against the direction of rotation(Mustafa et al., 2015). The figure below shows the major stress causing factors in a rotating fan;

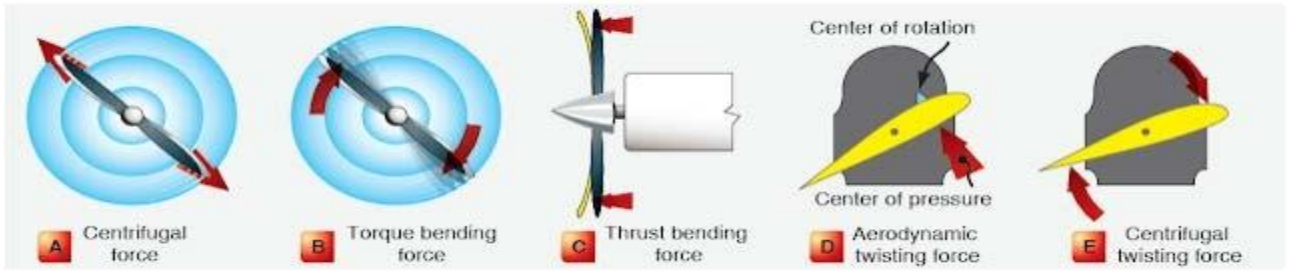


Fig 4.2: Stress causing factors in rotating fan.

For our analysis purposes we've estimated an averaged value of 100 N/cm^2 (1 MPa) centrifugal force. The centrifugal force is generally a function of radius and rotation velocity which vary with position along the blade span. A separate analysis has been made for the 86 N thrust bending force. The results have initially been evaluated individually and then the effect of their superposition has been analyzed. This allows us to isolate the major stress contributing force so that the design can be suitably reinforced if required.

Stress Analysis Procedure and Results

The stress analysis has been performed in Comsol Multiphysics 5.1 under a Structural Mechanics study. The application mode used is the 3D solid Stress-Strain application mode. The equilibrium equations for the model are as follows;

$$\begin{aligned}
 -\frac{\partial \sigma_x}{\partial x} - \frac{\partial \tau_{xy}}{\partial y} - \frac{\partial \tau_{xz}}{\partial z} &= F_x \\
 -\frac{\partial \tau_{xy}}{\partial x} - \frac{\partial \sigma_y}{\partial y} - \frac{\partial \tau_{yz}}{\partial z} &= F_y \\
 -\frac{\partial \tau_{xz}}{\partial x} - \frac{\partial \tau_{yz}}{\partial y} - \frac{\partial \sigma_z}{\partial z} &= F_z
 \end{aligned}$$

F represents the body forces, while the subscript represents the direction in which they act.

The equation can succinctly be represented as $-\nabla\sigma = \mathbf{F}$ where σ represents the stress tensor consisting of three normal stresses and 6 shear stresses. The shear stresses are symmetrical. The stress tensor is shown below;

$$\begin{array}{ccc}
 & & \text{In the stress matrix} \\
 \left[\begin{array}{ccc}
 \sigma_{xx} & \tau_{xy} & \tau_{xz} \\
 \tau_{yx} & \sigma_{yy} & \tau_{yz} \\
 \tau_{zx} & \tau_{zy} & \sigma_{zz}
 \end{array} \right] & \longrightarrow & \begin{array}{l}
 \tau_{xy} = \tau_{yx} \\
 \tau_{yz} = \tau_{zy} \\
 \tau_{zx} = \tau_{xz}
 \end{array}
 \end{array}$$

The stress-strain and then strain-displacement relations are substituted in the equation so that the equation can be expressed in the form of displacement and is known as Navier's Equation.

The elasticity matrix \mathbf{D} relates the stress and strain.

$$\begin{bmatrix} \sigma_{xx} \\ \sigma_{yy} \\ \sigma_{zz} \\ \sigma_{yz} \\ \sigma_{zx} \\ \sigma_{xy} \end{bmatrix} = \frac{E}{(1+\nu)(1-2\nu)} \begin{bmatrix} 1-\nu & \nu & \nu & 0 & 0 & 0 \\ \nu & 1-\nu & \nu & 0 & 0 & 0 \\ \nu & \nu & 1-\nu & 0 & 0 & 0 \\ 0 & 0 & 0 & 1-2\nu & 0 & 0 \\ 0 & 0 & 0 & 0 & 1-2\nu & 0 \\ 0 & 0 & 0 & 0 & 0 & 1-2\nu \end{bmatrix} \begin{bmatrix} \varepsilon_{xx} \\ \varepsilon_{yy} \\ \varepsilon_{zz} \\ \varepsilon_{yz} \\ \varepsilon_{zx} \\ \varepsilon_{xy} \end{bmatrix}$$

D, the elasticity matrix

The strain components can be expressed in the form of displacements in the x, y and z direction. The displacements are expressed as u, v, w for x, y, z directions respectively. The relations are shown below;

$$\begin{array}{ll}
 \varepsilon_{xx} = \frac{\partial u}{\partial x} & \varepsilon_{yz} = \frac{1}{2} \left(\frac{\partial v}{\partial y} + \frac{\partial v}{\partial z} \right) = \varepsilon_{zy} \\
 \varepsilon_{yy} = \frac{\partial v}{\partial y} & \varepsilon_{zx} = \frac{1}{2} \left(\frac{\partial u}{\partial z} + \frac{\partial w}{\partial x} \right) = \varepsilon_{xz} \\
 \varepsilon_{zz} = \frac{\partial w}{\partial z} & \varepsilon_{xy} = \frac{1}{2} \left(\frac{\partial v}{\partial x} + \frac{\partial u}{\partial y} \right) = \varepsilon_{yx}
 \end{array}$$

A static analysis has been performed since the stresses are likely to be invariable with time. Solving the **partial differential equations (PDEs)** generated yields the solution to the static problem.

A single fan-blade has been isolated; since all the fan blades are geometrically same and experience the same forces, the results for each blade is likely to be similar. The 3D isolated fan-blade has been imported in COMSOL. The material selected is carbon epoxy fiber composite with transverse fibers. This is a conscious choice since no axial force acts in the transverse direction hence carbon fibers are less likely to fail since carbon fibers are brittle and brittle materials generally fail under tensile and compressive stresses instead of shear stresses. The carbon fiber properties as mentioned below:

Material Properties:

Properties	Carbon
Density (kg/m³)	1800
Young's Modulus (Pa)	17 x 10 ¹⁰
Poisson's Ratio	0.23
Tensile Yield Strength	14 x 10 ⁸
Tensile Ultimate Strength	14 x 10 ⁸

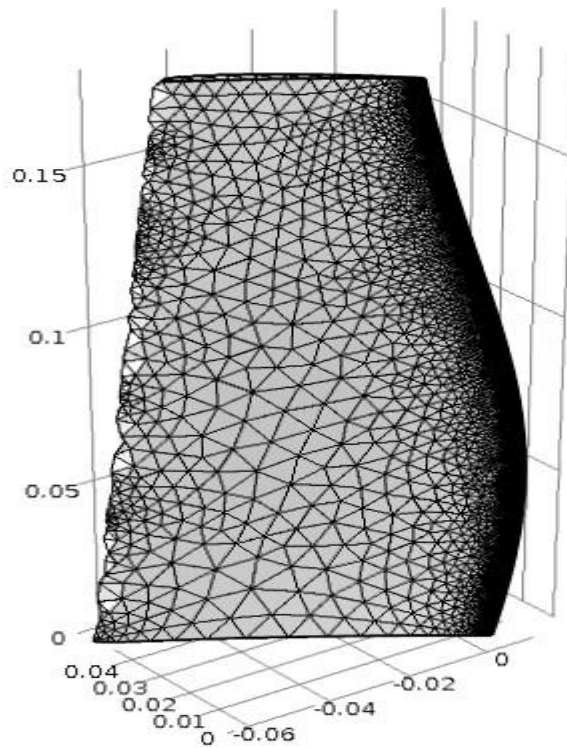
Table 9: Material Properties

The hub end of the fan blade was fixed and the respective forces and stresses were applied on their respective surfaces. A suitably sized tetrahedral mesh was generated to capture the smallest sections of the airfoil in detail.

The mesh parameters and the generated mesh are displayed below:

Element Size Parameters	
Maximum element size:	<input type="text" value="0.0179"/> m
Minimum element size:	<input type="text" value="0.00062"/> m
Maximum element growth rate:	<input type="text" value="1.5"/>
Curvature factor:	<input type="text" value="0.6"/>
Resolution of narrow regions:	<input type="text" value="0.5"/>

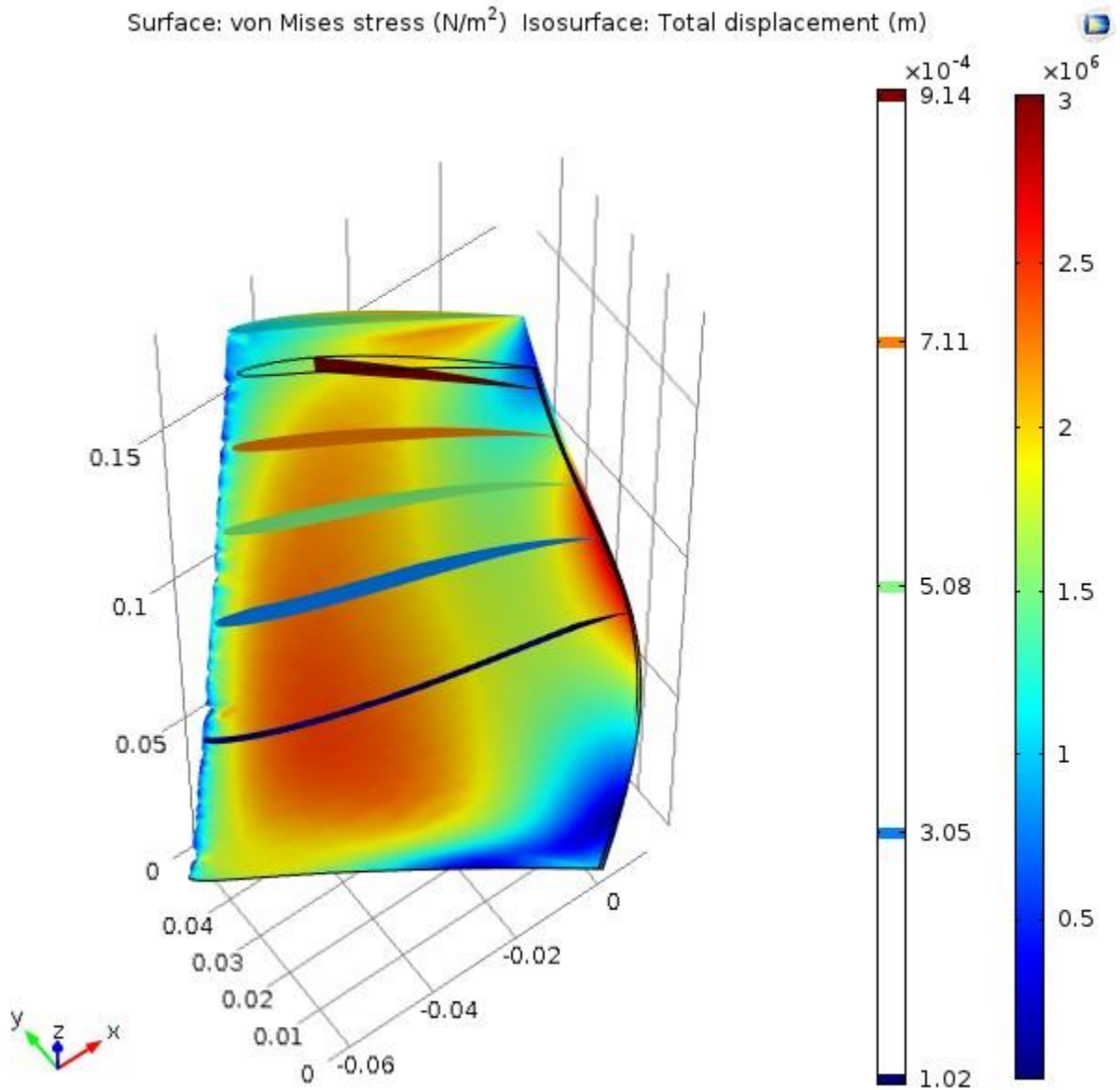
Mesh parameters



Generated Mesh

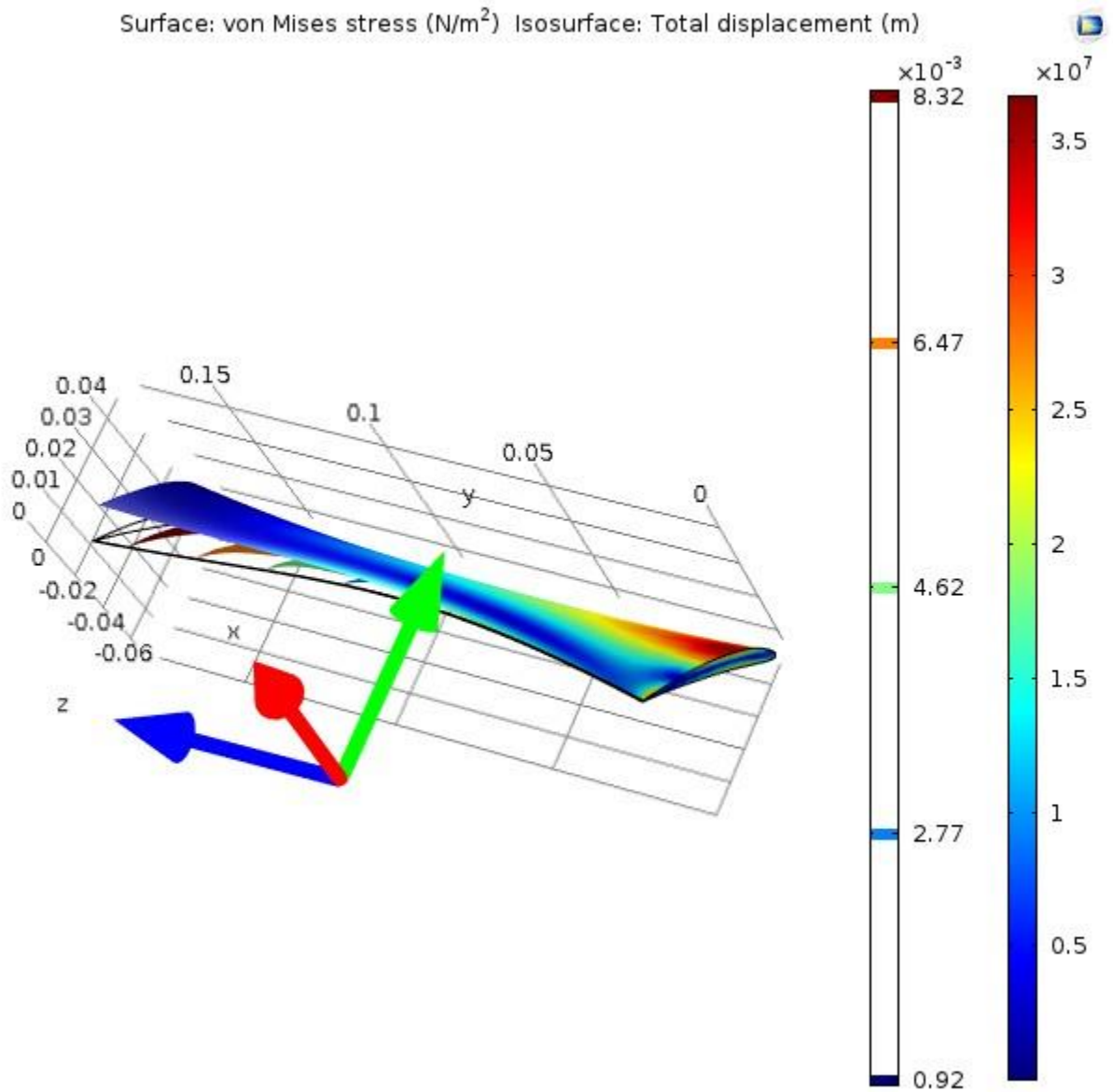
Once the mesh was generated, a Structural Mechanics study was run. Stress results were produced and iso-surfaces were produced to highlight deflection.

Results for Centrifugal Force



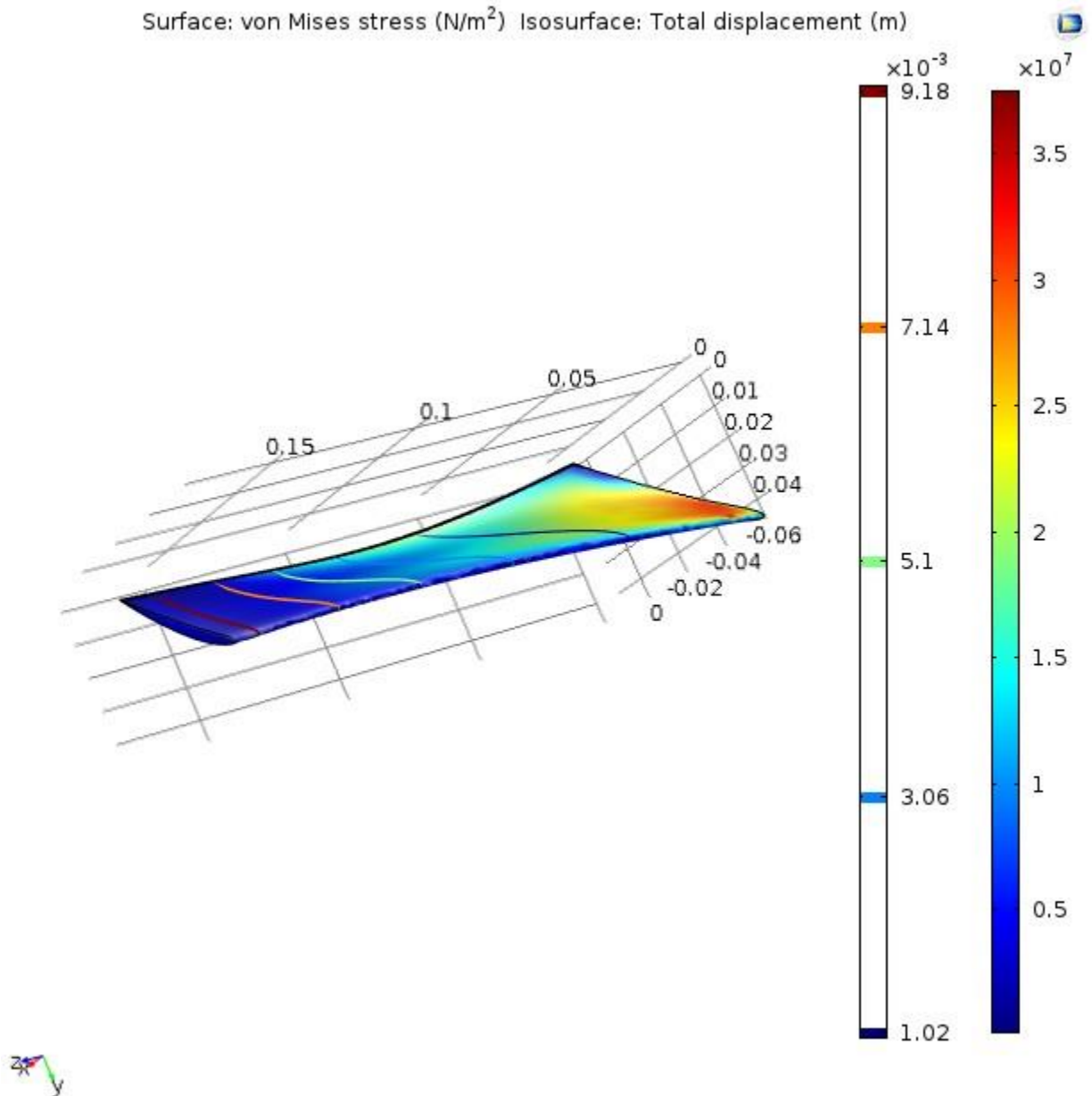
The snapshot displays the stress and the displacement as a result of the centrifugal force.

Results for Thrust Force



The snapshot highlights the stress and deformation as a result of the thrust force

Superposed Results



Snapshot shows the stress and deformation results when both centrifugal force and thrust force have been applied

Analysis of Results

Forces	Maximum Stress (Pa)	Maximum deformation (m)
Centrifugal Force	$3 \cdot 10^6$	$9.14 \cdot 10^{-4}$
Thrust Force	$3.5 \cdot 10^7$	$8.32 \cdot 10^{-3}$
Centrifugal & Thrust	$3.5 \cdot 10^7$	$9.18 \cdot 10^{-3}$

Table 10 : Stress and Deformation Analysis

The results indicate thrust to be the major stress causing force causing a maximum stress of 35MPa. Most of the deformation is also as a result of thrust (almost 10 times as much as the centrifugal force). The combined maximum stress is approximately the same as that experienced with thrust alone. Since carbon fiber has a tensile yield strength of 1.4 GPa, the design is well within safe structural requirements even after incorporating stress concentration and safety factors. The maximum stress occurs at the hub end of the fan blade and at the corners/edges of the wing blade.

The deflection is greatest at the tip end of the fan blade. A maximum deflection of 9.18 mm is expected near the tip, as highlighted by iso-surfaces of the airfoil along the span of the fan-blade. The deflection produced as a result of stresses is likely to slightly deform the fan blades over time and use which will result in changes in the thrust results in future operation. The deformation is likely to change the angle of twist ϕ over time while also affecting the geometric spline connecting the hub and tip airfoils.

CHAPTER 5: CONCLUSION AND RECOMMENDATION

1. Conclusion

The results of the CFD analysis clearly show that the optimum design selected for the fan blades is appropriate to produce the desired values of thrust required for this project. The two airfoils selected, provide the most suitable combination for blade design. The stresses on the fan blades are negligible and well within the range of the material's yield and tensile strengths. The difference between theoretically calculated thrust (94 N) and the thrust from the CFD analysis (86 N) is not significant. The sensitivity analysis revealed Setting angle Θ seems to be the most important parameter while optimizing the fan design. Also the analysis revealed that different parameters in conjunction with each other produce better thrust values; for example airfoils **NACA 5407 (tip) and NACA 7410 (root)** produce a much greater thrust (86N) when paired with a higher setting angle Θ , than when the setting angle is lower (43N thrust). The analysis further reveal that the stresses tend to concentrate near the hub (maximum Stresses of 35MPa) and hence the choice to choose a thicker airfoil at the root.

The results show that the designed ducted fan is an improvement on the market purchased axial fan if thrust production is the only metric on which to base our decision. Since the engine is to be used in a drone, thrust enhancement opens up the possibility of carrying out heavier objects as well as accommodating increased capacity of fuel tank. If the drone is to be used for agricultural purposes such as fertilizing and seed dropping, it can serve greater area per journey. The design is sustainable and scalable as it can be suitably scaled by using the drone in conjunction with electrical and

programmed control systems to perform various operations remotely and with minimal human involvement. The design is efficient and can be improved and performs adequately at the given constraints (thrust requirements and stress resilience). However, since the design has complicated airfoils generated from joining hundreds of points with curves generated from specific equations, manufacturing it requires CNC machines capable of achieving a great degree of precision and accuracy. The CNC's should also be able to operate with carbon fibers. As off now, the mentioned manufacturing capabilities are limited in Pakistan. A few Defence organizations have the required machinery and expertise to manufacture fan blades with sufficient precision and accuracy. There is further room for investigation. The final word can only be given once the fan is manufactured and tested on a test bench under the given conditions. Improvement and optimization within this design can then be decided based on evidence shown by the testing results of the fan.

2. Recommendations

There are some changes that can be made to further improve the design:

- The investigation has focused on thrust optimization while disregarding efficiency, load resilience and various other metrics. Moving forward, fan design can be optimized keeping a compromise between thrust, efficiency and these various other requirements.
- Angle of attack can be changed by selecting a different combination of airfoils
- Blade twist angle can be varied to find the optimum twist for minimization of swirl velocity component. The number of airfoil sections along the span of the fan blade can be varied and the angle of twist varied slowly while moving from one section to another.
- Research can be extended on how to manufacture customized fan blades in Pakistan at an economically viable cost.

REFERENCES

- [1] Dixon S. L. (1998), Fluid Mechanics and Thermodynamics of Turbomachinery (4th Edition).
- [2] Osborne William C. (1977), Fans 2nd Edition.
- [3] Ramsden, K. W. (2008), Course Notes for Axial Compressor Design and Performance.
- [4] Bleier, Frank P. (1998), Fan Handbook: Selection, Application, and Design.
- [5] Strohmeyer, H. (2009), Improving the Efficiency of an Industrial Low Speed Fan.
- [6] Eck, Bruno (1973), FANS Design and Operation of Centrifugal, Axial Flow and Cross Flow Fans, Pergamon Press.
- [7] King Tech Turbines, Product Catalog (retrieved from URL):
http://www.kingtechturbines.com/products/index.php?main_page=product_info&product_s_id=3
- [8] Munson R., Young F., Okiishi H., Huebsch W. (2012) Fundamentals of Fluid Mechanics, 6th Edition, John Wiley and Sons Inc.
- [9] Hibbeler R.C., (2011) Mechanics of Materials, 8th Edition, Pearson.
- [10] Schubel P., Crossley R. (2012) Wind Turbine and Blade Design Review, Wing Engineering, p. 365-388.

Research Papers References

Blaho, M. (1975). Optimum Design of Axial Flow Fans With Cambered Blades of Constant

- Thickness. *Periodica Polytechnica Mechanical Engineering*, 19(2), 79–89.
- Chahine, C., Verstraete, T., & He, L. (2015). Multidisciplinary Design Optimization of an Aero-Engine Fan Blade with Consideration of Bypass and Core Performance. *Proceedings of the 11th World Congress on Structural and Multidisciplinary Optimization*, June, 5–10.
- D. Almazo; C. Rodríguez; M. Toledo. (2013). Selection and Design of an Axial Flow Fan. *Journal of Mechanical, Aerospace, Industrial, Mechatronic and Manufacturing Engineering*, Vol.7, N°5, 7(5), 923–926. <https://waset.org/publications/15827/selection-and-design-of-an-axial-flow-fan>
- De Ryck, H. (2008). Turbofan design for the commercial aircraft. *MS Thesis*, May, 1–98.
- Huang, C. H., & Gau, C. W. (2012). An optimal design for axial-flow fan blade: Theoretical and experimental studies. *Journal of Mechanical Science and Technology*, 26(2), 427–436. <https://doi.org/10.1007/s12206-011-1030-7>
- Kumar, S., & Bartaria, V. N. (n.d.). *a Review of Literature on Design of Axial Flow Fan*. 109–113.
- Mustafa, E., Danardono, Triyono, Anggono, A. D., & Ahmed, A. A. (2015). Finite element analysis and optimization design of aluminium axial fan blade. *ARP Journal of Engineering and Applied Sciences*, 10(16), 7288–7292.

APPENDIX I: AIR PROPERTIES AT DIFFERENT ALTITUDES

Geo potential Altitude above Sea Level - h - (m)	Temperature - t - (°C)	Acceleration of Gravity - g - (m/s ²)	Absolute Pressure - p - (10 ⁴ N/m ²)	Density - ρ - (10 ⁻¹ kg/m ³)	Dynamic Viscosity - μ - (10 ⁻⁵ N s/m ²)
-1000	21.50	9.810	11.39	13.47	1.821
0	15.00	9.807	10.13	12.25	1.789
1000	8.50	9.804	8.988	11.12	1.758
2000	2.00	9.801	7.950	10.07	1.726
3000	-4.49	9.797	7.012	9.093	1.694
4000	-10.98	9.794	6.166	8.194	1.661
5000	-17.47	9.791	5.405	7.364	1.628
6000	-23.96	9.788	4.722	6.601	1.595
7000	-30.45	9.785	4.111	5.900	1.561
8000	-36.94	9.782	3.565	5.258	1.527
9000	-43.42	9.779	3.080	4.671	1.493
10000	-49.90	9.776	2.650	4.135	1.458
15000	-56.50	9.761	1.211	1.948	1.422
20000	-56.50	9.745	0.5529	0.8891	1.422
25000	-51.60	9.730	0.2549	0.4008	1.448
30000	-46.64	9.715	0.1197	0.1841	1.475
40000	-22.80	9.684	0.0287	0.03996	1.601
50000	-2.5	9.654	0.007978	0.01027	1.704
60000	-26.13	9.624	0.002196	0.003097	1.584
70000	-53.57	9.594	0.00052	0.0008283	1.438
80000	-74.51	9.564	0.00011	0.0001846	1.321